

Bonding in Pentalene Complexes and Recent Applications.

F. Geoffrey N. Cloke,^a Jennifer C. Green*^{†,b} Alexander F. R. Kilpatrick*,^c
Dermot O'Hare^c

^a *Department of Chemistry, School of Life Sciences, University of Sussex, BN1 9QJ, UK*

^b *Department of Chemistry, University of Oxford, Inorganic Chemistry Laboratory, South Parks Road, Oxford OX1 3QR, UK*

^c *Department of Chemistry, University of Oxford, Chemistry Research Laboratory, Mansfield Road, Oxford OX1 3TA, UK*

[†] Corresponding author jennifer.green@chem.ox.ac.uk

Contents

1. Introduction
 2. Pentalene and its dianion
 3. Coordination modes of pentalene complexes
 4. η^8 -mode of bonding
 - 4.1 Structural studies of η^8 -pentalene complexes
 - 4.2 Bonding in η^8 -pentalene complexes
 - 4.2.1 Bis(η^8 -pentalene) compounds
 - 4.2.2 Mono(η^8 -pentalene) derivatives
 - 4.3 Examples of η^8 -pentalene derivatives
 5. η^5, η^5 mode of bonding
 - 5.1 Structural studies of η^5, η^5 -pentalene complexes
 - 5.2 Bonding in η^5, η^5 -pentalene complexes
 - 5.2.1 Bis(η^5, η^5 -pentalene) bimetallic complexes
 - 5.2.2 Mono(η^5, η^5 -pentalene) bimetallic derivatives
 6. Other bonding modes
 7. Small molecule activation
 8. Catalysis
 9. Intermetallic communication
 - 9.1 Electronic delocalisation in pentalene-bridged complexes
 10. Conclusions
- Abbreviations

Figure Titles

References

Abstract

Molecular orbital (MO) theory is used to describe the bonding in transition metal pentalene complexes in a variety of its coordination modes. The various MO models account for structural parameters and lead to simple rules for electron counting in pentalene complexes. Applications of pentalene complexes in small molecule activation, catalysis and electronic coupling are reported.

Keywords

Pentalene
Bonding
Metallocene
Nanowires
Catalysis
CO₂ activation

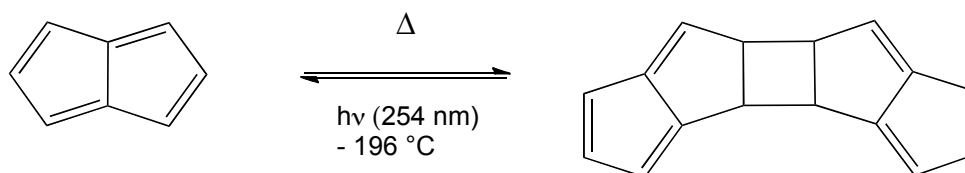
1. Introduction

In the last 20 years the use of pentalene as a ligand in transition metal organometallic chemistry has become more frequent. The broad areas in which its complexes have found application have been small molecule activation, catalysis and as models for conducting polymers in materials chemistry. Previous articles have reviewed the syntheses and structures of pentalene complexes[1, 2] and described bonding in reported and hypothetical complexes in the context of their electron numbers.[3] In this article we present bonding models for pentalene complexes in a variety of its coordination modes and review certain aspects of their chemical and physical properties.

2. Pentalene and its dianion

Early speculation suggested pentalene might possess aromatic character.[4] Prediction of its polyolefinic nature,[5] subsequently confirmed by MO calculations, has been verified experimentally.[6] Pentalene, C₈H₆, is an eight carbon molecule that can be considered as the double-ring fused relative of cyclopentadiene, or as cyclooctatetraene with a 1,5-transannular bond. The

neutral species is an 8π Hückel anti-aromatic hydrocarbon with a double-bond alternant C_{2h} structure, and the molecule has only been isolated in matrices at very low temperatures.[6] Neutral pentalene is unstable above $-196\text{ }^{\circ}\text{C}$ and undergoes a rapid Diels-Alder reaction to the [2+2] dimer (Scheme 1).[7] Introduction of bulky substituents inhibits dimerisation, such that hexaphenyl pentalene[8] and 1,3,5-tri-*t*-butyl pentalene have both been isolated at room temperature.[9]



Scheme 1 Dimerisation of neutral pentalene.[7]

In contrast the dianionic form, $[\text{C}_8\text{H}_6]^{2-}$, is a 10π aromatic species and is consequently thermally stable at room temperature. The pentalenyl dianion has been crystallographically characterised as a dilithiated dimethoxyethane (DME) adduct $[\text{Li}(\text{DME})]_2\text{Pn}$,[7] and the carbocycle shows D_{2h} symmetry, with lithium ions in an η^5, η^5 -coordination mode on opposite faces of the planar pentalene ring.

The π symmetry MO of $[\text{C}_8\text{H}_6]^{2-}$ are represented in Fig. 1 together with those of $[\text{C}_8\text{H}_8]^{2-}$. The ten π electrons occupy up to π_5 , which is non-bonding. The orbitals principally involved in covalent bonding to metals are π_4 and π_5 , which lie close in energy. The closely related orbitals of the cyclooctatetrene dianion, $[\text{C}_8\text{H}_8]^{2-}$, are degenerate; the formation of the transannular bond in pentalene imparts bonding character to π_4 and lowers it in energy with respect to π_5 . In contrast π_3 is raised in energy compared to π_2 and becomes of suitable energy to mix with metal orbitals.

Fig.1 Comparison of the π symmetry orbitals of $[\text{C}_8\text{H}_8]^{2-}$ with those of $[\text{C}_8\text{H}_6]^{2-}$. The HOMO is π_5 . [10]

3. Coordination modes of pentalene complexes

When acting as a ligand with transition metals pentalene has a maximum of 8 bonding electrons, L_3X_2 function in a neutral counting scheme,[11, 12] and shows a variety of multihaptic bonding modes (Fig. 2).

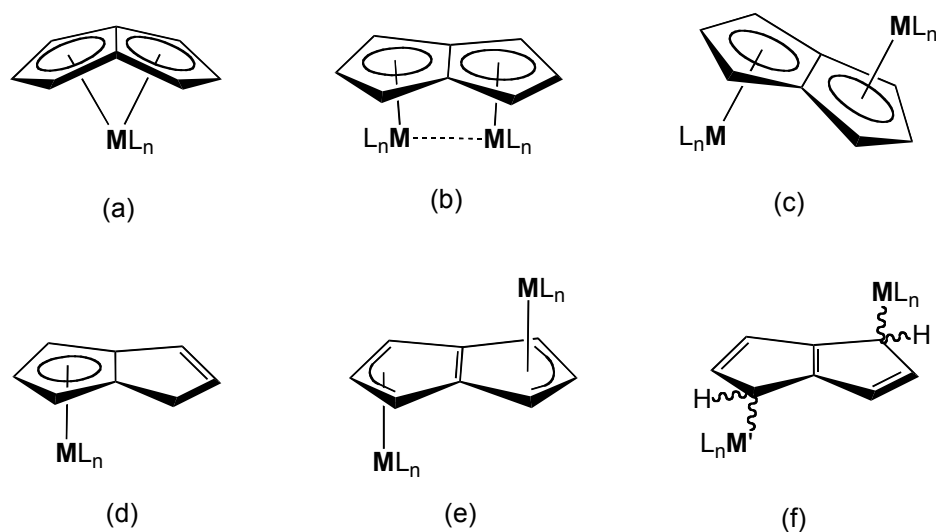


Fig. 2 Examples of the coordination modes of pentalene ligands.

4. η^8 -mode of bonding

4.1. Structural studies of η^8 -pentalene complexes

The η^8 -mode, in which all eight carbons are involved in bonding to the metal (Fig. 2(a)), leads to a folding of the ligand about its C–C bridgehead bond towards the metal centre. This is commonly encountered in pentalene complexes with f- and early d-block elements, as the 'umbrella'-like effect of the folded ligand aids the steric stabilisation of the metal centres.[1] This distortion from planarity is accompanied by a loss of aromaticity, and is quantified by the 'fold angle' (Fig. 3(a)), which is dependent on both steric and electronic factors.

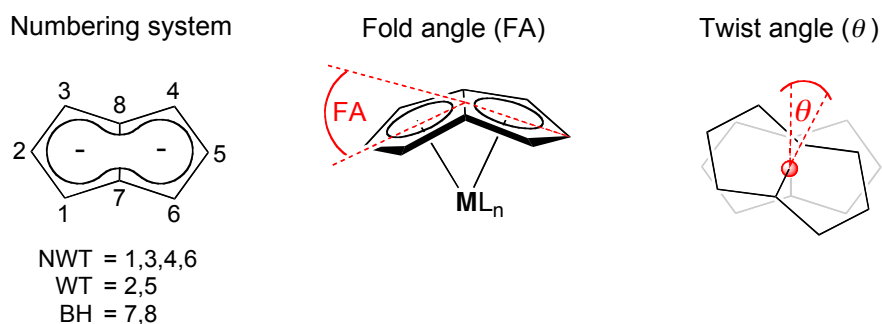


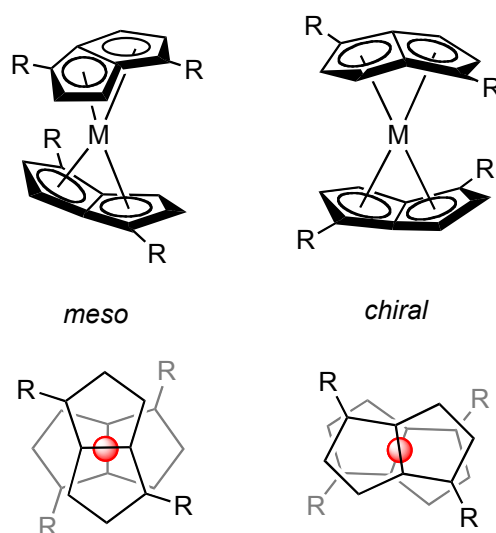
Fig. 3. Pentalene numbering system and geometric parameters for an η^8 -bound pentalene complex (a) fold angle, FA (b) twist angle, θ , for bis(pentalene) complexes.

In general, for complexes with a given ligand set the FA may be simply related inversely to the size of the central metal.[1] For example, (η^8 -Pn)MCp complexes show a marked increase in fold angle from M = Ti (37.0°) to V (43.0°) in accordance with the decreasing ionic radii (0.670 vs 0.640 Å respectively for 6-coordinate M^{3+} ions).[13] However comparing the series of Group 4 permethylpentalene complexes Pn^*MCpCl and Pn^*MCp_2 for M = Ti, Zr, Hf,[14] the titanium and hafnium species have near identical FAs, despite the considerably larger size of Hf^{4+} (0.71 Å) relative to Ti^{4+} (0.605 Å).[14] O'Hare and co-workers attributed this to the more diffuse nature of the atomic orbitals for the 3rd row transition metal leading to better orbital overlap with Pn^* , which compensates for the loss in aromaticity as the ligand folds away from planarity.[14] Within a series of complexes bearing the same metal and pentalene ligand, the FAs increase as electron deficiency at the metal centre increases. For example, the mononuclear tantalum(V) complexes (η^8 - Pn^+) $TaCl_xMe_{3-x}$ for $x = 0-3$, which show a small but discernable increase in FA as the number of electron withdrawing chloride ligands increases.[15] Furthermore, the electronic properties of the pentalene ligand itself have an effect on FA, as first shown by comparison of the FAs for (η^8 -Pn)ZrCpCl (33.0°)[16] and (η^8 - Pn^*)ZrCpCl (30.7°),[14, 17] which provides evidence for the enhanced donor ability of the permethylated ligand.

The structural characterisation of permethylpentalene analogues MPn^*_2 (M = Zr, Hf) has been reported recently,[18] revealing greater average M–Ct (Ct = ring centroid) than those for other Group 4 Pn^* complexes (distances range from $2.080(2)$ to $2.135(1)$ Å),[14, 19] attributed to the greater steric demand of two Pn^* ligands preventing closer approach to the metal center. The C–C distances and the fold angle about the carbon skeleton in MPn^*_2 are in good agreement with those predicted for MPn_2 , despite the extra inductive effect of the methyl groups on Pn^* . However, the twist angle, θ , between the Pn^* ligands ($41.6(5)$ Zr; $42.8(6)$ Hf) is less staggered than the predicted values, again reflecting the steric demand of Pn^* . It is expected that a steric clash between the methyl group on the wingtip (WT, C2/C5 in Fig. 3) position, with the bridgehead (BH, C7/C8) carbon

on the other pentalene ligand, would move the energetic minimum of the HOMO to a lower twist angle.

The actinide bis(pentalene) compounds have been reported for $M = \text{Th}$; $\text{Pn}' = \text{Pn}^+$ and $M = \text{U}$; $\text{Pn}' = \text{Pn}^+, \text{Pn}^*$. [20, 21] For the silylated complexes the 1,4 substituents on the ligand act as a conformational lock and render the stereochemistry complex. Two isomers were found within the same crystal and reflect two non-interconvertible species of meso (S_4) and chiral (D_2) symmetries in which the faces of the ligands are bound on opposing sides (Scheme 2). The bulky silyl groups are found in almost identical locations in both forms and dictate the crystal packing. [20] Twist angles are 83° for the meso form and 38° for the chiral form.



Scheme 2. Diastereomers of $M(\eta^8\text{-Pn}^+)_2$. [20]

The permethylated complex UPn^*_2 exists as three stereochemical isomers in the solid state, [21] a staggered conformation and two eclipsed conformations which differ in the angle between the mean planes of the metal and the WT carbon atoms for the two Pn^* ligands.

4.2 Bonding in η^8 -pentalene complexes

4.2.1 Bis(η^8 -pentalene) compounds

Bis(pentalene) sandwich compounds where the pentalene ligand is octahaptic have been characterised for Ti, Zr, Hf, [16] Ce [22, 23] Th [20] and U. [20, 21] The d-block Group 4 $M(\eta^8\text{-Pn})_2$ compounds lack X-ray structural data but low temperature NMR studies suggest a D_2 structure. [24] Calculations employing the

RHF method and LANL2DZ basis sets confirm a D_2 structure for $ZrPn_2$ and $HfPn_2$ with a 50° twist angle, θ , between the bridgehead vectors. Ti is found to have a C_1 global minimum lying only $2 \text{ kcal}\cdot\text{mol}^{-1}$ below a nearby D_2 conformation.[24] DFT calculations (BP86/TZP) are in agreement with a predicted θ of 55° . [3]

Table 1. Bis(η^8 -pentalene) complexes

Group	CBC class[11, 25]	Compound	Ref
3	ML_7X_3	$[MPn^*_2]^-$; M = Sc, Y.	[26]
4	ML_6X_4	MPn'_2 ; M = Ti, Zr, Hf; $Pn' = C_8H_5(2-R)$, R = H, Me	[16]
		MPn^*_2 ; M = Ti, Zr, Hf	[18]
f-block	ML_7X_3	$[CePn^\dagger_2]^-$	[22]
	ML_6X_4	MPn^\dagger_2 ; M = Ce, Th, U	[20, 22]
		MPn^*_2 ; M = Ce, U	[21, 23]

The 20 valence electron (VE) count of the Group 4 pentalene sandwiches aroused theoretical interest.[27] The RHF study presents a correlation diagram between the two more symmetrical structures of D_{2h} ($\theta = 0^\circ$) and D_{2d} ($\theta = 90^\circ$) symmetry with the minimum D_2 structure lying in between (Fig. 4). The HOMO, an out of phase combination of the two π_5 orbitals (Fig. 5), is non-bonding at the two extremes. On relative rotation of the two ligands the symmetry distinction between π_4 and π_5 is lost and the HOMO is stabilised by favourable overlap with a metal d orbital in the intermediate conformation. The PE spectra of the triad consists of two sets of three bands in the low IE range in good agreement with the spacing of the orbitals given by the calculation.[24]

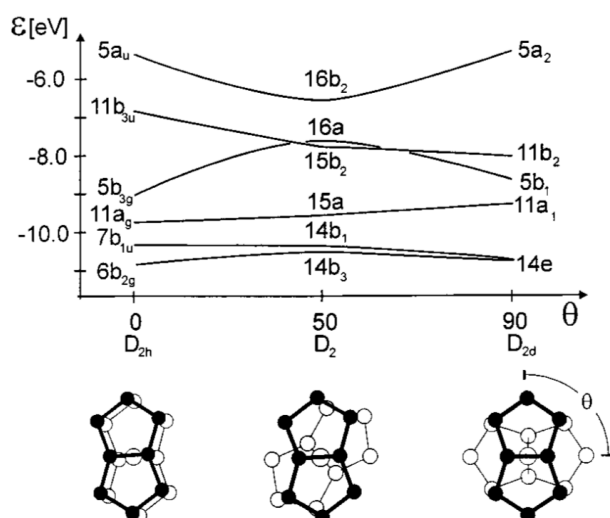


Fig. 4 Correlation diagram of the six highest occupied orbitals of Pn_2Ti as function of θ .
Reproduced with permission from [24]

DFT calculations (BP86/TZP) were carried out on the parent unsubstituted compounds ThPn_2 and UPn_2 . [28] For ThPn_2 a D_2 conformation was found to be $3 \text{ kJ}\cdot\text{mol}^{-1}$ more stable than a D_{2h} conformation. A comparable calculation for ZrPn_2 indicates a larger difference of $28 \text{ kJ}\cdot\text{mol}^{-1}$. [10]

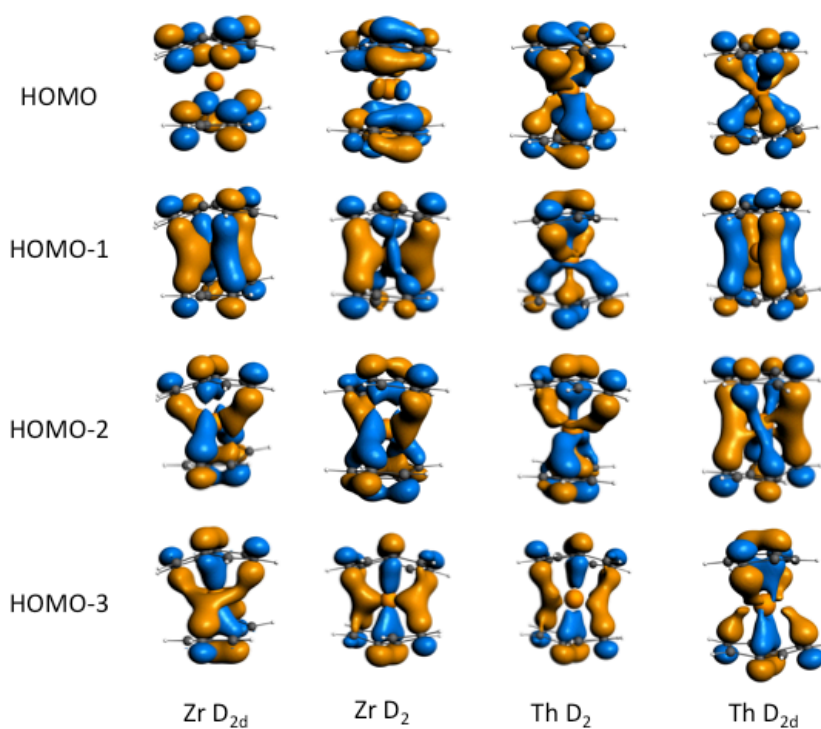


Fig. 5. Frontier orbitals of ZrPn_2 and ThPn_2 with D_{2d} and D_2 symmetry. [10]

Fig. 5 shows that for ThPn_2 , with D_{2d} symmetry, the HOMO is stabilised by overlap with the $5f(z(x^2-y^2))$ orbital, the calculation indicating a 14% 5f contribution. The HOMO-1 has a 24% contribution from the $6d(x^2-y^2)$ orbital, a more effective stabilising interaction similar to that found for thoracene.[29] The 5f/6d percentage contributions to the HOMO-2 and HOMO-3 are 6/9 and 2/13 respectively. The ability of the actinides to employ 5f orbitals in bonding leads to the two conformations having a trivial energy difference. A D_{2h} structure is destabilised by the close proximity of the wingtip hydrogens.

The presence of two isomers leads to the PE spectra of ThPn^{\dagger}_2 and UPn^{\dagger}_2 to be less well resolved than those of the d-block analogues. He II spectra of UPn^{\dagger}_2 clearly show a band assigned to ionisation of the two 5f electrons at 5.79 eV a significantly lower energy than that of uranocene at 6.2 eV.[29, 30] It has a similar value to that of octamethyl uranocene (5.73 eV).[31]

Cerium also forms bis(pentalene) complexes, CePn^{\dagger}_2 , [22] and CePn^*_2 [23] analogous to cerocene, CeCOT_2 , for which the ground state electronic structure has been subject of much debate and interest. A potassium salt of the anion, $[\text{CePn}^{\dagger}_2]^-$ has also been characterised.[22] X-ray diffraction studies of CePn^{\dagger}_2 identified two isomers with twist angles, θ , of 85° and 33° for the Ce(IV) compound. The Ce(III) anion which has longer metal-ring distances has an isomer close to eclipsed with a twist angle of 10° and another with a twist of 44° . The permethylated complex CePn^*_2 , in common with its uranium analogue UPn^*_2 , displays three relative orientations of the ligands in the solid state, one staggered ($\theta = 79.8^\circ$) and two skewed ($\theta = 40.1^\circ$ and 20.1°), which probably exist in dynamic equilibrium.

DFT calculations[22, 23] on CePn_2 and CePn^*_2 with D_{2d} symmetry suggest an electronic structure very similar to ThPn_2 . However, the electronic structure of the CeCOT_2 analogue has proved controversial.[32] The system can be viewed as a complex of a closed-shell Ce(IV) ion sandwiched by two aromatic annulene dianions and bonded with a significant Ce 4f-ring covalency, or as a Ce(III) ion with an almost atomic-like $4f^1$ subconfiguration, coupled to the unpaired electron in the ring's highest energy occupied π -orbitals. It is likely that a similar situation pertains for CePn_2 . The Ce 4f orbitals are radially contacted and, as with

a hydrogen dimer H_2 at a stretched bond distance, the $^1\text{A}_{1g}$ ground state is not best described by a single determinant MO model; configuration interaction gives a better description. A recent study by Dolg *et al.* using relativistic quantum chemical *ab initio* methods best describes CePn_2 as a Ce(III) system in which the Ce 4f orbitals are involved in a weak Ce-ring interaction, which corresponds to an elongated covalent bond and gives rise to the multi-reference character of the system.[33]

X-ray absorption near-edge structure (XANES) studies at the K-edge for CePn^{\dagger}_2 [22] and L(III)-edge for CePn^*_2 [23] indicate a charge on Ce intermediate between Ce^{3+} and Ce^{4+} . For CePn^*_2 post-edge structure enables an estimate of the Ce 4f content, the value being 0.87 ± 0.05 . Both compounds have low energy charge transfer bands associated with small HOMO-LUMO gaps. In addition they show temperature independent paramagnetism (TIP) and unusual ^1H and ^{13}C NMR shifts which are attributed to the TIP.

4.2.2 Mono- η^8 -pentalene derivatives

Treating a $\text{M}(\eta^8\text{-Pn})$ fragment with C_{2v} symmetry (Fig. 6) enables description of its frontier orbitals which may be used for binding further ligands.

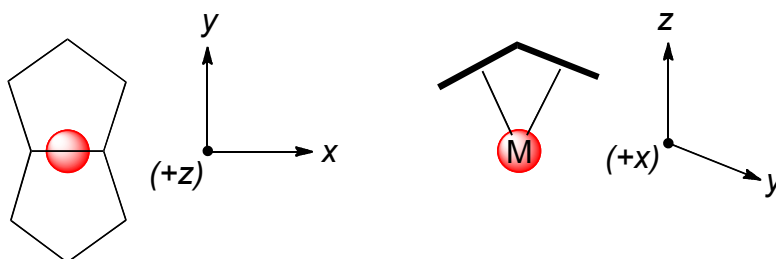


Fig. 6. Definition of Cartesian coordinates for a C_{2v} $\text{M}(\eta^8\text{-Pn})$ fragment.

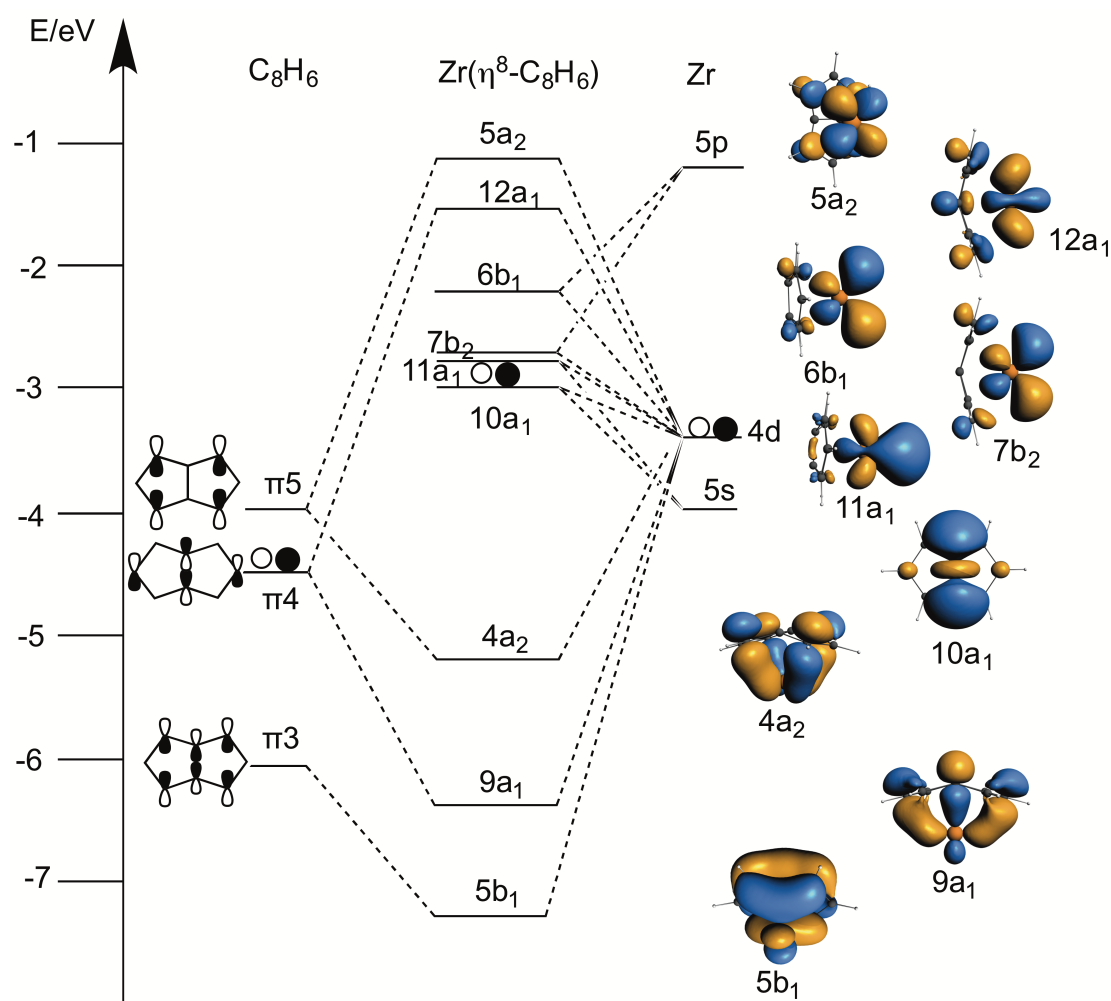
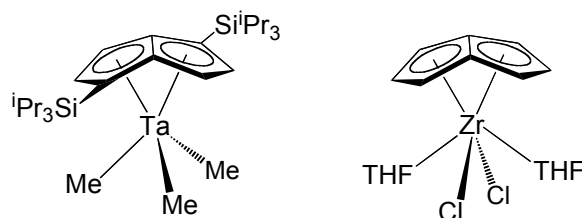


Fig. 7. Energy levels and isosurfaces for the Kohn-Sham frontier orbitals of $\text{Zr}(\eta^8\text{-Pn})$ with C_{2v} symmetry.

The pentalene orbitals $\pi 5$ and $\pi 4$ are the principal means of bonding to the metal forming the MO $9a_1$ and $4a_2$; the unoccupied orbitals $12a_1$ and $5a_2$ are their antibonding counterparts. $\pi 3$ also makes a smaller contribution to form $5b_1$ with the consequence that the largely metal based orbital $6b_1$ is also raised in energy. The largely metal based frontier orbitals available for binding further ligands are $10a_1$, $11a_1$, $7b_2$ and $6b_1$. Comparison of the frontier orbitals of $\text{M}(\eta^8\text{-Pn})$ with those of a bent metallocene (MCp_2) unit is of interest. The orbitals $10a_1$ and $11a_1$ resemble the two a_1 symmetry orbitals of a bent metallocene but the third orbital $7b_2$ lies perpendicular to the plane containing the metal and the two bridgehead carbons, the equivalent of the metallocene plane, whereas a bent metallocene has the lowest three frontier orbitals lying within this plane.[34-36] The fourth frontier orbital of MPn , $6b_1$, lies within this plane, very close in energy to $7b_2$. We

may therefore anticipate different coordination modes for $M(\eta^8\text{-Pn})$ than MCp_2 . The three outward directed orbitals, $11a_1$, $7b_2$ and $6b_1$ suggest, when considering d-block transition metals, that trigonal coordination will be more favoured for $M(\eta^8\text{-Pn})$ than the planar coordination found for MCp_2 . Use of all four frontier orbitals leads to square-pyramidal coordination.

In compounds of the type $M(\eta^8\text{-Pn})\text{X}_3$, where M is a group 4 metal, the two X ligands lie in the equivalent of the metallocene plane. The symmetric combination of the X frontier σ orbitals use the $M(\eta^8\text{-Pn})$ $11a_1$ orbital for bonding to the metal, the lower lying orbital of a_1 symmetry. The alternative disposition with the X ligands in the plane of the metal and WT carbons has poor orbital with the $11a_1$ orbital and is constrained to use the higher energy $12a_1$ orbital for bonding.



Scheme 3. Examples of trigonal[15] and pyramidal[16] coordination by $M(\eta^8\text{-Pn})$.

Compounds in which the metal atom shows η^8 coordination of pentalene are found for early d-block transition metals and f-block elements (Table 2).

Table 2. Examples of compounds with η^8 coordination of pentalene to a single metal.

Group	CBC class	Compound	Ref
Group 2	ML_7X_2	$\text{Pn}'\text{Ba}(\text{THF})_4$; $\text{Pn}' = \text{dibenzopentalene-(1,4-SiMe}_3)_2$	[37]
Group 3	ML_5X_3	Pn^+ScCp^* $\text{PnScCp}'(\text{THF})$; $\text{Cp}' = \text{Cp, Cp}^*, \text{Ind.}$ $[\text{Pn}^+\text{Sc}(\text{THF})(\mu\text{-Cl})]_2$ $[\text{Pn}^+\text{Y}(\text{THF})(\mu\text{-I})]_2$	[38] ^a [39] [38] [1]
Group 4	ML_3X_3	$(\text{Pn}^+\text{Ti})_2(\mu\text{-O})$	[40, 41]
	ML_3X_4	Pn^*TiR_2 ; $\text{R} = \text{Me, CH}_2\text{Ph}$ $\text{Pn}^*\text{M}(\text{CH}_2\text{Ph})_2$; $\text{M} = \text{Zr, Hf}$	[42] [42] [43]

		$(Pn^+Ti)_2(\mu-O)_2$ $(Pn^+Ti)_2(\mu-S)_2$ $(Pn^+Ti)_2(\mu-NPh)_2$	[40, 41] [38, 44]
	ML_4X_4	$[Pn^*Hf(CH_2Ph)_3]^-$ $[Pn^*M(Ph)_3]^-$; M = Zr, Hf.	[18] [18]
	ML_5X_3	$Pn'TiCp$; $Pn' = C_8H_5(2-R)$, R=H, Me. $[Pn^+Ti(py)(\mu-Cl)]_2$ $[Pn^*TiCl(\mu-Cl)]_2$ $[Pn^*M(\mu-Cl)_{3/2}]_2(\mu-Cl)_2Li \cdot THF_x$; M=Zr, Hf. $(Pn^*Zr)_2(\mu-CH_2)(\mu-Me)_2$	[16] [38] ^b [19] [19] [18]
	ML_5X_4	$Pn'MCpX$; M=Ti, Zr; $Pn' = C_8H_5(2-R)$, R=H, Me; X=Cl, Br. $Pn^*MCp_{2-x}Cl_x$; M = Ti, Zr Hf; x = 0, 1. Pn^*MCp^*Cl ; M = Ti, Zr, Hf. $Pn^*MCp'X$; M = Ti, Zr; $Cp' = Cp, Cp^{Me}$, Cp^{tBu} , Cp^{nBu} , Cp^{Me3} , Ind; X = Cl, Me. $PnZrCl_2(THF)_2$ $Pn'Zr(\eta^3\text{-allyl})_2$; $Pn' = Pn, Pn^*$. $Pn^*Ti(\kappa^2-O_2CR)_2$; R = Me, CH_2Ph . $Pn^*M(\kappa^2-O_2CCH_2CHCH_2)_2$; M = Zr, Hf. $PnZr(Ind)Cl$	[16] [14] [14] [45] [16] [18, 46] [42] [46] [39]
	$M_2L_9X_7$	$[Pn^+Ti]_2(\mu-Cl)_3$	[47]
Group 5	ML_5X_3	$Pn'VCp'$; $Pn' = C_8H_5(2-R)$, R = H, $Cp' = Cp, Cp^*$; R = Me, $Cp' = Cp$.	[48]
	ML_3X_5	$Pn'TaCl_3$; $Pn' = C_8H_4(SiMe_3\text{-}1,5)_2$ $[Pn^+TaCl(\mu-CH_2)]_2$, $Pn^+TaCl_xMe_{3-x}$; x = 0–3.	[49] [15]
f-block	ML_6X_2	$Pn^+Yb(THF)_3$	[1]
	ML_5X_3	Pn^+UCp^* $Pn^+U(\kappa^3\text{-}Tp^{Me2})$ $Pn^+SmCp^*, (\eta^8\text{-}Pn^+)Sm(\eta^5\text{-}Pn^+H)$	[50] [51] [52]

	ML ₅ X ₄	[Pn ⁺ M(μ-Cl) ₂] ₄ ; M=Th,U. [Pn*U(μ-Cl) ₄][Li(TMEDA)] ₂ ,	[1] [53]
	ML ₆ X ₄	[Pn*UCp(μ-Cl) ₂][Li(TMEDA)]; Cp' = Cp, Cp*. [Pn ⁺ UCp*] ₂ (μ-η ² :η ² -N ₂)	[53] [50]
	ML ₇ X ₄	Pn*UCp ₂	[53]

^a CCDC 1502468

^b CCDC 1502469

Sandwich compounds featuring both a pentalene and a cyclopentadienyl ring have been characterised for both Group 4 and Group 5 d-block elements. The 11a₁, 7b₂ and 6b₁ orbitals provide a good match to the three occupied π orbitals of a cyclopentadienyl ring. (η⁸-Pn)VCp, first synthesised by Jonas[48] provides the 18 electron archetype. The electronic structure of this complex, calculated by Saillard,[27] is in good agreement with the experimental data. The two d electrons are housed in orbital 7b₁ which back donates to both ligands (Fig. 8).

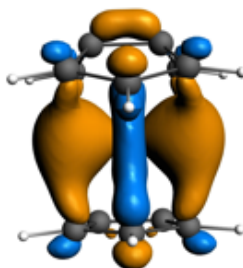


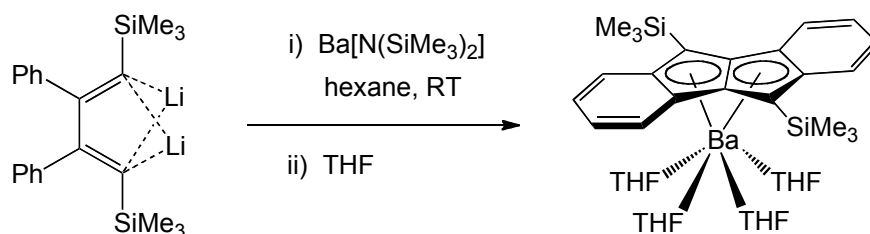
Fig. 8. Isosurface for the HOMO of (η⁸-Pn)VCp.[10, 27]

(η⁸-Pn)TiCp has one unpaired electron in a similar orbital. It is oxidised by dichloroethane and dibromoethane to form the halide derivatives (η⁸-Pn)TiCpX, X = Cl, Br,[16] the TiPn fragment utilising all four frontier orbitals in this case.

Outside the d-block, mono(η⁸-Pn⁺) complexes have been reported for the lanthanide metals in the +2 oxidation state, YbPn⁺(THF)₃,[1] and +3 oxidation state, (η⁸-Pn⁺)SmCp*[52] and (η⁸-Pn⁺)Sm(η⁵-Pn⁺H).[52]

The uranium(III) mixed-sandwich complex (η⁸-Pn⁺)UCp* has been characterised and shown to bind dinitrogen reversibly[50]. Such small molecule activation is discussed in Section 7.

Xi and co-workers recently reported the synthesis of $\text{Pn}'\text{Ba}(\text{THF})_4$, $\text{Pn}' = \text{dibenzopentalene-(1,4-SiMe}_3)_2$, the first example of main-group metal bound in an η^8 -coordination mode, by reaction of phenyl substituted 1,4-dilithio-1,3-butadiene with $\text{Ba}[\text{N}(\text{SiMe}_3)_2]_2$ (Scheme 4).[37]



Scheme 4. Synthesis of a barium complex with a η^8 -dibenzopentalenide ligand.[37]
A survey of characterised compounds (Tables 1 and 2) indicates that valence requirements of the metal are an important factor in determining the stability of $\eta^8\text{-Pn}^\dagger$ compounds.

5. η^5, η^5 mode of bonding

5.1 Structural motifs in η^5, η^5 -pentalene complexes

When two metals are bonded to a single pentalene ligand one particular point of interest is the degree to which the metals are placed centrally with respect to the two rings. The degree of slip is measured by the geometric parameter Δ , defined in Fig. 9. Another important structural parameter for η^5, η^5 -bound pentalene ligands is the hinge angle (HA), which is a measure of the deviation from planarity of the C5 rings. This is defined as the angle between the plane of the WT carbon and NWT carbons and the plane of the NWT carbons and the BH carbons (Fig. 9).

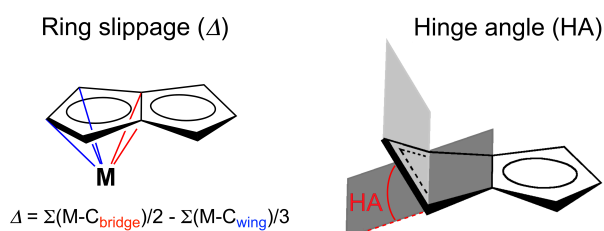


Fig. 9. Definition of geometric parameters for ring slippage (Δ) and hinge angle (HA).

Double-sandwich compounds of the general formula $M_2(\eta^5, \eta^5\text{-Pn}')_2$ (Fig. 10) have been synthesised for a wide range of d-block transition metals (Table 3).

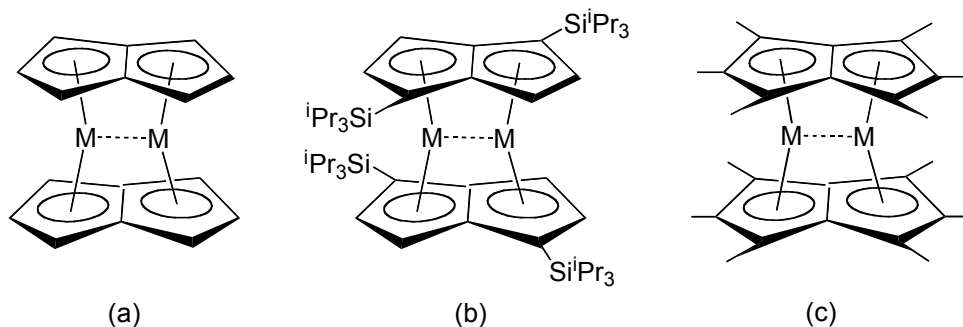


Fig. 10. Examples of di-metal bis(pentalene) double-sandwich complexes.

Table 3. Examples of bis(η^5, η^5 -pentalene) di-metal complexes, $M_2(\eta^5, \eta^5\text{-Pn}')_2$.

Pentalene	CBC	Metal	Reference
Pn		Co	[54]
		Ni	[55]
Pn [†]	ML ₄ X ₄	Ti	[47]
	ML ₄ X ₄	Cr	[56]
	ML ₄ X ₄	Mo	[57]
	ML ₄ X ₄	Mo/W	[58]
		Rh	[59]
	ML ₂ X ₂	Pd	[59]
Pn [*]	ML ₄ X ₅	V	[60]
	ML ₄ X ₄	Cr	[60]
	ML ₄ X ₃	Mn	[60]
	ML ₄ X ₂	Fe	[61]
		Co	[60]
	ML ₂ X ₂	Ni	[60]

The double-sandwich complexes based on Pn^{*} provide a more straightforward series with which to study the variation in structural parameters across the transition series (Table 4).

Table 4. Experimental and calculated metal spin states (M_S , M_S), distances (\AA), slippage (Δ , \AA), fold angle (FA, $^\circ$) and calculated bond order for $M_2Pn^*_2$. [60, 61]. Calculated values are in *italics*.

M	V	Cr	Mn	Fe	Co	Ni
S	0, 0	0, 0	1, 1	1, 1	0, 0	0, 0
M–M	2.169 <i>2.12</i>	2.150 <i>2.15</i>	2.277 <i>2.27</i>	2.3175 <i>2.36</i>	2.491 <i>2.56</i>	2.569 <i>2.68</i>
av. C–C	1.442 <i>1.45</i>	1.449 <i>1.45</i>	1.448 <i>1.45</i>	1.4464 <i>1.45</i>	1.447 <i>1.45</i>	1.441 <i>1.45</i>
av. M–C	2.262 <i>2.29</i>	2.1695 <i>2.19</i>	2.160 <i>2.17</i>	2.1258 <i>2.15</i>	2.129 <i>2.15</i>	2.191 <i>2.25</i>
Δ	0.0555 0.0463 <i>0.02</i>	0.0842 0.0925 <i>0.06</i>	0.1316 0.1488 <i>0.11</i>	0.147 0.154 <i>0.16</i>	0.0895 0.3672 <i>0.06, 0.37</i>	0.2770 0.2500 <i>0.35</i>
FA	2.89 2	0.70 4	1.18 7	0.8 2	2.04 5	2.76 5
M–M bond order	<i>2.83</i>	<i>1.98</i>	<i>1.13</i>	<i>0.26</i>	<i>-0.59</i>	<i>0.03</i>

The spin states are in stark contrast to those of the MCp^*_2 series apart from $M = Mn$. The M–C distance shows a decrease across the period apart from a rise at Ni. This can presumably be attributed to the increase in nuclear charge causing a decrease in size of the metal with some additional antibonding feature in the case of Ni. The M–M distance however shows an increase across the period, with the exception of a marginal decrease from V to Cr. These features are discussed below.

5.2 Bonding in bis(η^5, η^5 -pentalene) bimetallic complexes

When two metal atoms are sandwiched between two pentalene ligands the proximity of the two fused five membered rings of a ligand ensures that there will be an interaction between the metal atoms. Thus there is the potential to support metal-metal multiple bonding that is not commonly found.

Saillard *et al.* have reported results from geometry optimizations of $M_2Pn'_2$ species for $M = Cr-Ni$ and $Mo-Pd$, [3] and Green *et al.* for $M = Mo$, [62] Ti [40, 47], V-Ni [60, 61] and Rh, Pd [59]. Figure 11a shows an MO scheme for

V_2Pn_2 with D_{2h} symmetry, built from V_2 and Pn fragments. (The running numbers on the MO symmetry labels are chosen to enable easy comparison between Pn and Pn^* derivatives.) Figure 11b gives isosurfaces of the Kohn-Sham orbitals with >10% V occupancy.

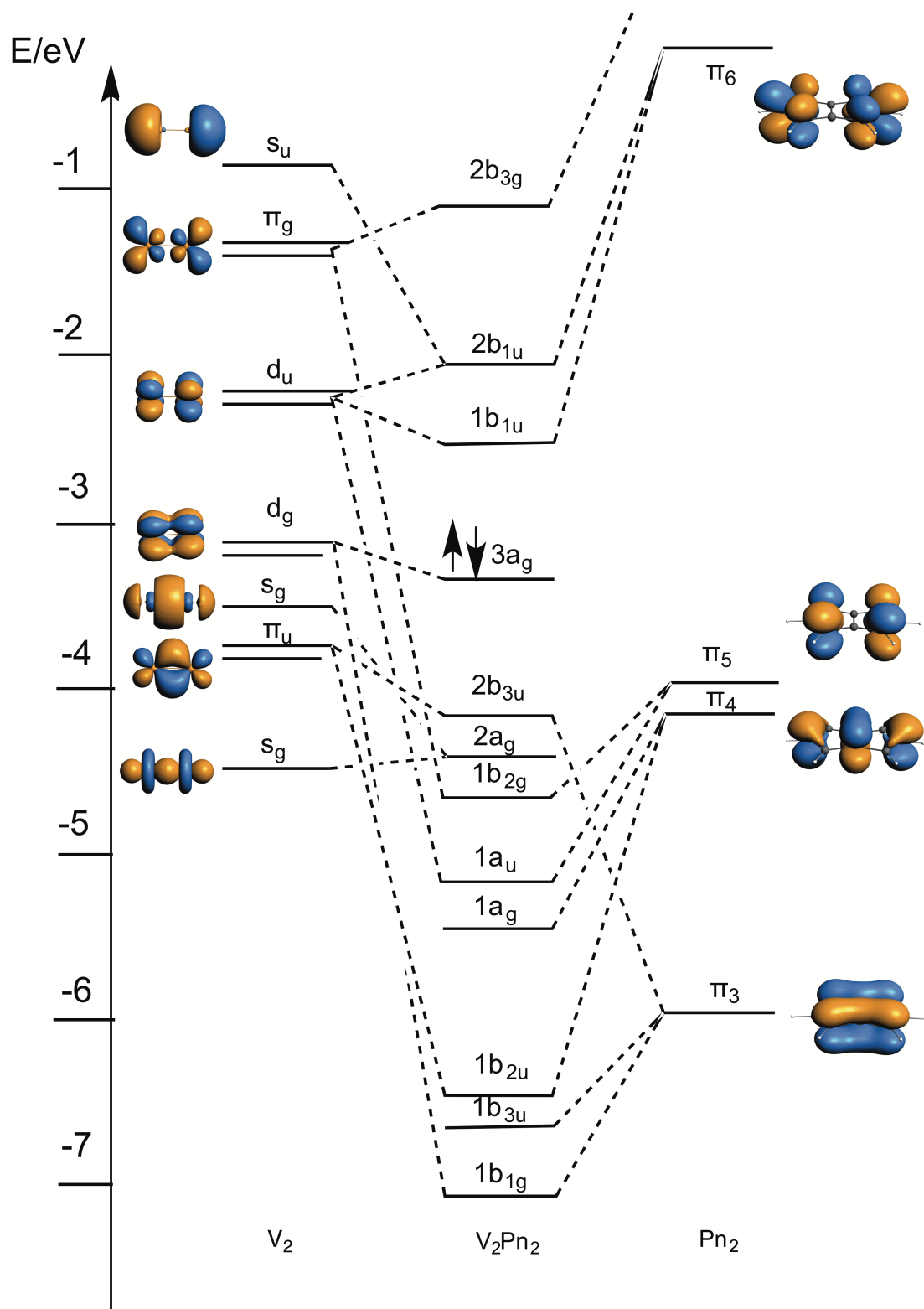


Fig. 11a. MO scheme for V_2Pn_2 built from V_2 and Pn fragments.[10]

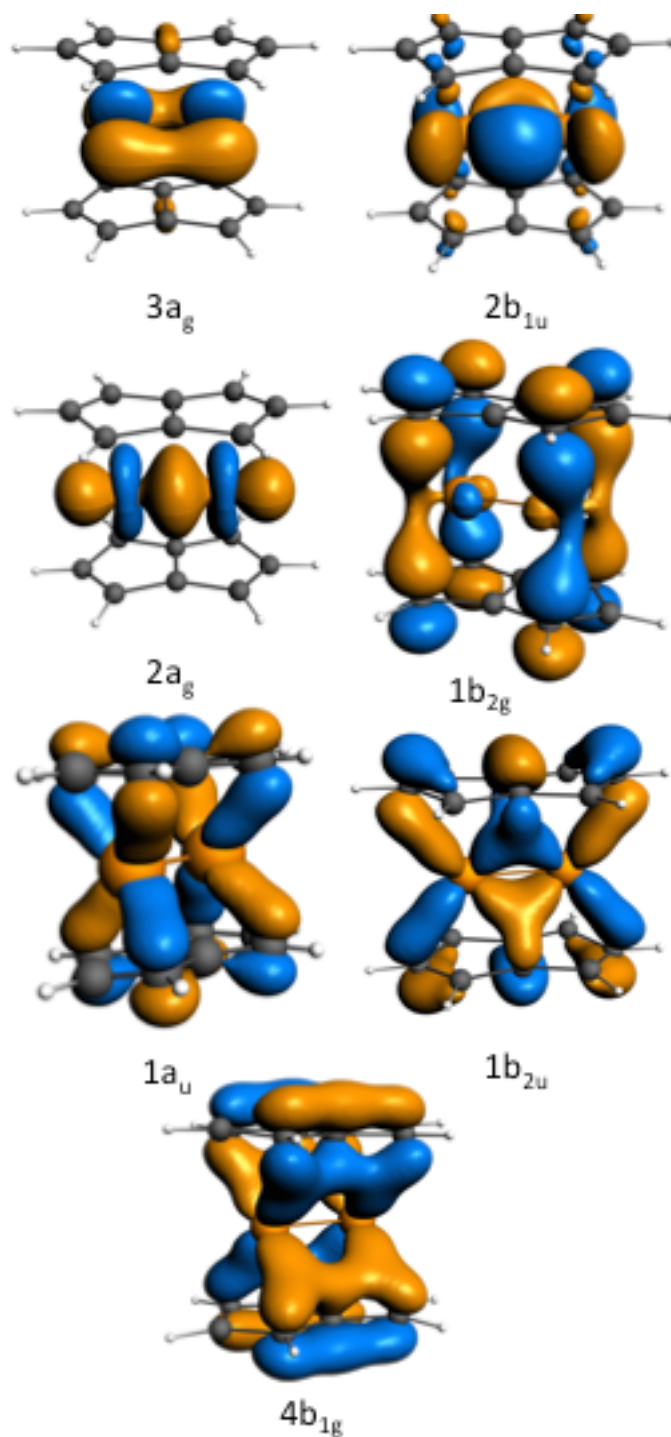


Fig. 11b. Isosurfaces for occupied orbitals of V_2Pn_2 with greater than 10% V occupancy.[10]

The highest three occupied orbitals derive directly from V-V σ , π and δ bonding orbitals and demonstrate a triple bond between the V atoms. Good overlap between π_5 and a V-V δ^* orbital, π_4 and a V-V π orbital and π_3 and a V-V δ orbital produce bonding MOs with 31%, 32% and 23% V content respectively.

For Ti_2Pn_2 with D_{2h} the $3a_{1g}$ orbital is unoccupied and the $2b_{2u}$ orbital is the HOMO. However this is not an energy minimum and the more stable structure has C_{2v} symmetry with an angle subtended at Ti by the opposing ring centroids of 153° . [40, 47] The Ti–Ti distance is calculated as 2.37 Å, a reasonable value for Ti–Ti double bond. Structural parameters of this model compound are in good agreement with the X-ray crystallographic data for $\text{Ti}_2\text{Pn}^{\dagger}_2$. [47] The high energy Ti–Ti bonding electrons, the presence of a low lying unoccupied metal based orbital and the open structure lead to considerable reactivity for $\text{Ti}_2\text{Pn}^{\dagger}_2$ discussed in section 7.

The most complete series of M_2Pn_2 double-sandwiches is M_2Pn^*_2 for $\text{M} = \text{V-Ni}$. [60, 61]. Fig. 12 shows the trend in orbital energies for this series across the first row transition metals and isosurfaces for the additional occupied orbitals. [60] As the nuclear charge of the metal increases the metal based orbitals are stabilised. From Cr to Co those orbitals which are occupied in addition to those of V_2Pn^*_2 are all metal-metal antibonding so there is a general increase in M–M distance across the series.

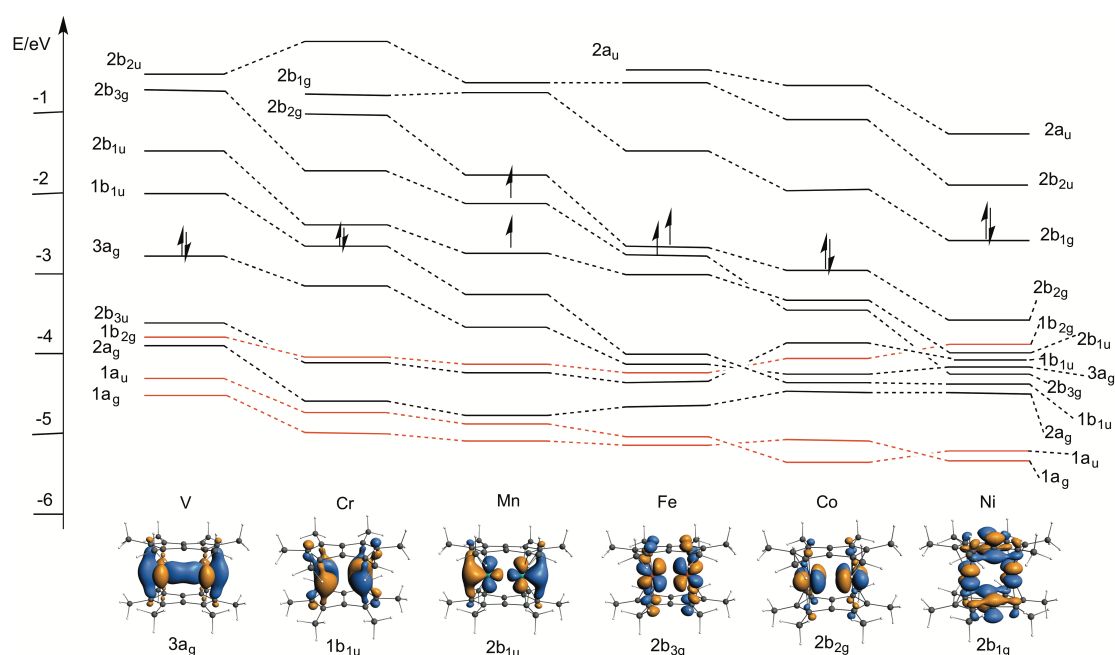


Fig. 12. MO energy levels for M_2Pn^*_2 ($\text{M}=\text{V-Ni}$) showing trend across the series and additional MO isosurfaces. [10, 60, 61]

For $\text{M} = \text{Cr}$ calculations predict a singlet ground state with a triplet state lying 0.22 eV higher in energy, in agreement with experimental observations. Magnetic studies shown a similar singlet triplet ordering for $\text{Cr}_2\text{Pn}^{\dagger}_2$ but in this

case DFT and CASPT2 calculations place the triplet state marginally below the singlet.[56] In all cases the energy differences are found to be within the accuracy of the calculations. The Cr compounds have a metal-metal bond order of 2. The molybdenum dimer $\text{Mo}_2\text{Pn}^\dagger_2$ has a diamagnetic ground state[57] with two electrons occupying the $1b_{1u}$ HOMO.[62] There is a double bond between the Mo atoms with one σ and one π component the latter lying in the plane parallel to the ligand planes. PES supports the calculated orbital structure.[62]

For $M = \text{Mn}$ a triplet state ($S = 1$) is calculated to lie 0.44 eV below a singlet state. The bond order again decreases and Mn_2Pn^*_2 has a bond order of one. However, $\text{Mn}_2\text{Pn}^\dagger_2$ has a different structure,[63] in which one Mn is η^5 coordinated by both pentalenes, the other η^1 coordinated by both pentalenes (Fig. 13).

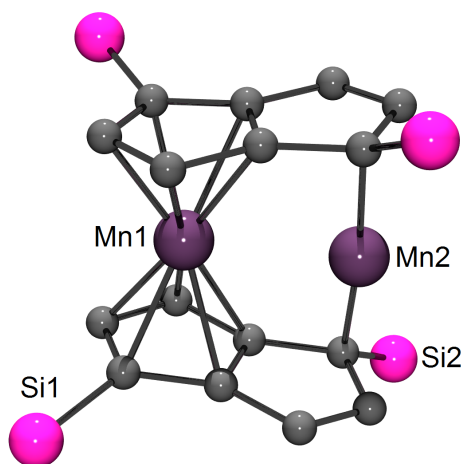


Fig. 13. Ball and stick diagram of solid-state structure of $\text{Mn}_2\text{Pn}^\dagger_2$, constructed from published coordinates.[63] H atoms and $i\text{Pr}$ groups omitted for clarity.

DFT calculations on Mn_2Pn_2 with various spin states give similar structures when $S = 3$ and $S = 2$ the $S = 3$ being the lower in energy by $4.7 \text{ kJ}\cdot\text{mol}^{-1}$. The $S = 3$ geometry is a better fit to the experimental structure. The magnetic measurements on $\text{Mn}_2\text{Pn}^\dagger_2$ are consistent with a $S = 3$ ground state and a thermally accessible $S = 2$ excited state. Analysis of the calculated spin density assigns a spin of 0.75 to the η^5 coordinated Mn and 2.25 to the η^1 coordinated Mn, the two overall spin states arising from ferromagnetic and antiferromagnetic coupling between the two Mn centres. Such a situation is reminiscent of the various spin states and coordination modes of Mn in a variety of

bis(cyclopentadienyl) manganese compounds. The difference between the two $\text{Mn}_2\text{Pn}'_2$ structures can be attributed to the greater ligand field strength of the Pn^* ligand compared with Pn^\dagger .

The di-iron double-sandwich complex initially proved elusive, but careful choice of starting materials enabled the synthesis of $\text{Fe}_2\text{Pn}^*_{\text{2}}$.^[61] The molecule has C_i symmetry in the solid-state structure, with slightly different Fe–Ct distances and an inversion centre between the two Fe atoms, whereas DFT calculations gave a D_{2h} structure as an energy minimum. The magnetic susceptibility data suggest that $\text{Fe}_2\text{Pn}^*_{\text{2}}$ has a well defined triplet ($S = 1$) configuration between 60 and 300 K consistent with the calculated ground state and half occupancy of the $2b_{3g}$ and $2b_{2g}$ orbitals. Fragment analysis afforded a decomposition of the bonding in terms of the MOs of the Fe dimer and the Pn^* ligand and enabled an estimation of the Fe–Fe bond order. The result was an order of 0.26, implying a weak but net favorable interaction between the two Fe atoms, but no Fe–Fe bond.

Whereas the $\text{M}_2\text{Pn}^*_{\text{2}}$ complexes from V, Cr and Mn optimise to D_{2h} symmetry for Co such a structure is a transition state and the energy minimum has C_{2h} symmetry with each Co tending towards η^5, η^3 coordination as is found experimentally. Fragment calculations indicate an antibonding interaction between the metals in this case with a bond order of (–0.59) consistent with the occupation of a further M–M antibonding orbital, $2b_{2g}$. Calculations on Rh_2Pn_2 also give a C_{2h} structure as the energy minimum but a D_{2h} model lies only 0.04 eV higher in energy.^[59] The solid state structure of $\text{Rh}_2\text{Pn}^\dagger_{\text{2}}$ shows a different distortion with the pentalene ligands twisted at 17.5° with respect to each other from an eclipsed configuration. As with the Co analogue there is an antibonding interaction between the Rh atoms with in this case both metal atoms significantly closer to the wingtip carbons than the bridgehead carbons.

The two additional electrons of $\text{Ni}_2\text{Pn}^*_{\text{2}}$ occupy orbital $2b_{1g}$ which is formally δ bonding between the Ni but is antibonding with respect to the bridgehead carbons, being the antibonding counterpart of bonding orbital $1b_{1g}$. Thus the Ni–C distance increases compared to that of the Co analogue and in this case both Ni atoms shift further toward the wingtip carbons although the formal Ni–Ni bond order is now zero. Calculations on Pd_2Pn_2 indicate a C_{2v} distortion

from D_{2h} symmetry but only as a gain of 0.01 eV. The solid state structure of $\text{Pd}_2\text{Pn}^{\dagger}_2$ obtained by X-ray crystallography suffered from disorder, but the Pd-Pd distance (2.786(2) Å) was in good agreement with the calculated values for the model species (2.868 and 2.871 Å for D_{2h} and C_{2v} structures respectively).[59]

In general the bonding models give an excellent account of the structural and magnetic features of these double-sandwiches. It serves as a guide as to the formalism with which to treat pentalene ligands when bonded to two metals. A total electron count for these molecules where pentalene is counted as donating eight electrons predicts an incorrect metal-metal bond order. If a formalism is adopted whereby the bridging carbons are counted as donating two electrons to each metal (Fig. 14), so each ring contributes five electrons to each metal then the metal forms metal-metal bonds of an order that satisfies the 18 electron rule in the cases of V, Cr, Mn and Fe as is shown in Fig 14. Also antibonding interactions are indicated for Co and Ni. The Ti double-sandwich lacks sufficient electrons to form a quadruple bond and obeys a 16 electron rule common for Ti compounds. Such an electron deficiency accounts in part for its exceptional reactivity discussed below.

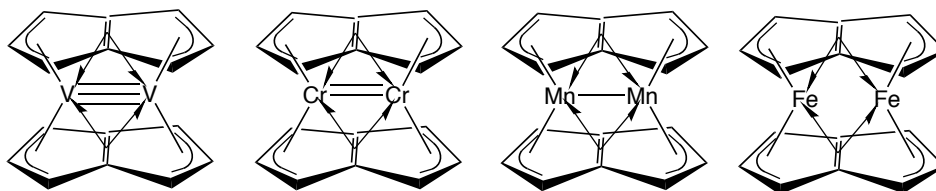


Fig. 14. M-M bond orders predicted by assuming that the bridging pentalene is a 5 electron L_2X donor to each metal; the allyl portion is an LX donor. The M-M bond orders predicted by this method are in accord with theory. Pentalene substituents are not shown for clarity. Adopted from ref [12].

5.3 Bonding in mono(η^5, η^5 -pentalene) bimetallic derivatives

Compounds in which two metals are coordinated to each of the five membered rings of a pentalene and also attached to other groups have either *syn*- or *anti*-configurations. They are mainly found for the later transition metals and are coordinated by groups such as carbonyl and cyclopentadienyl.

Table 5. Examples of mono(pentalene) bimetallic derivatives.

Group	CBC	Compound	Ref
5	ML_4X_5	<i>syn</i> -Pn(VCp) ₂	[64]

6		$\text{Pn}(\text{CrCp}^*_3)\text{O}$	[65]
7	ML_6X	$[\text{anti-Pn}(\text{M}(\text{CO})_3)_2]^{n-}; \text{M} = \text{Mn } n = 0, 1, 2; \text{Re } n = 0$ $\text{syn-Pn}(\text{M}(\text{CO})_3)_2; \text{M} = \text{Re}$	[66]
8	ML_4X_2	$\text{syn}-(\text{C}_8\text{H}_5\text{R})\text{Fe}_2(\text{CO})_5; \text{R} = \text{H}, \text{NMe}_2, \text{Ph.}$	[67-69]
	ML_4X_2	$\text{syn-Pn}^*\text{Fe}_2(\text{CO})_5$	[70]
	ML_4X_2	$\text{syn-Pn}(\text{Ru}(\text{CO})_2(\text{GeMe}_3))_2$	[71]
	ML_4X_2	$[\text{anti-Pn}(\text{MCp}^*)_2]^{n+}; \text{M} = \text{Fe, Ru}; n = 0, 1, 2$	[72, 73]
		$[\text{anti-Pn}^+(\text{FeCp}^*)_2]$	[74]
		$[\text{anti-Pn}^*(\text{MCp})_2] \text{ M} = \text{Co, Ni}$	[75]
		$[\text{anti-Pn}^*(\text{MCp}^*)_2] \text{ M} = \text{Fe, Co, Ni.}$	
9	ML_4X	$\text{syn-Pn}^*(\text{Co}(\text{CO})_2)_2$	[70]
	ML_4X	$[\text{anti-Pn}(\text{CoCp}^*)_2]^{n+}; n = 0, 1, 2$	[72]
	ML_4X	$\text{syn}-(\text{Pn}^*)(\text{M}(\text{CO})_2)_2; \text{M} = \text{Rh, Ir}$	[76]
10	ML_3X_2	$[\text{anti-Pn}(\text{NiCp}^*)_2]^{n+}; n = 0, 1, 2$	[72]
	ML_2X_2	$\text{anti-Pn}(\text{Ni}(\text{C}_3\text{H}_5))_2$	[77, 78]
f-block		$[\text{Cp}^*\text{Ln}(\text{THF})]_2(\mu\text{:}\eta^5, \eta^5\text{-Pn}^+); \text{Ln} = \text{Eu, Yb}$	[79]
		$[\text{Cp}^*\text{Ln}]_2(\mu\text{:}\eta^5, \eta^5\text{-Pn}^+); \text{Ln} = \text{Eu, Yb, Sm}$	[38, 80]

5.3.1 anti-bimetallic complexes

Some examples of *anti*-bimetallic complexes are shown in Fig. 15.

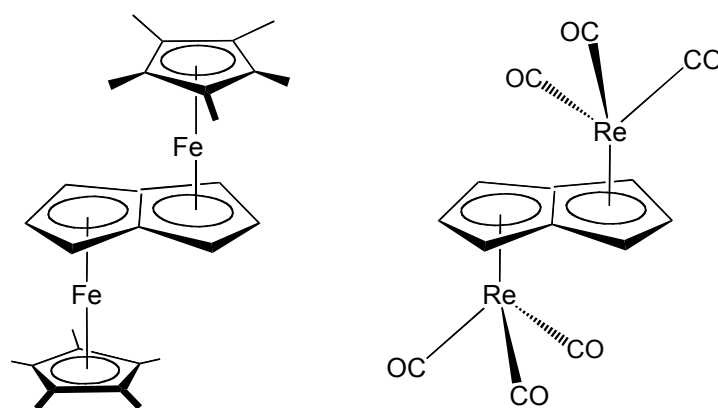


Fig. 15. Examples of *anti*-bimetallic pentalene complexes. [72, 73, 77, 78]

When two metals are placed on opposite sides of a pentalene ligand the bonding mode to the five membered ring appears to resemble that to a cyclopentadienyl

ligand, hence *anti*-Pn(Mn(CO)₃)₂ is analogous to CpMn(CO)₃, Pn(FeCp*)₂ is analogous to ferrocene and so forth. Thus the fragment M₂Pn presents six frontier orbitals for further bonding; the electron occupancy of these is metal dependent is 0 (Mn₂), 2 (Fe₂), 4 (Co₂) and 6 (Ni₂). The six MOs are equivalent to three trigonally disposed orbitals on each metal, hence each metal is isolobal with CH. The remaining twelve metal electrons occupy six orbitals, the equivalent of the a₁ and e₂ orbitals of ferrocene for each metal, often referred to as the “t_{2g}” set. Fig. 16 shows isosurfaces for these metal based orbitals. The t_{2g} sets may be employed for back donation to π acceptor ligands such as CO.

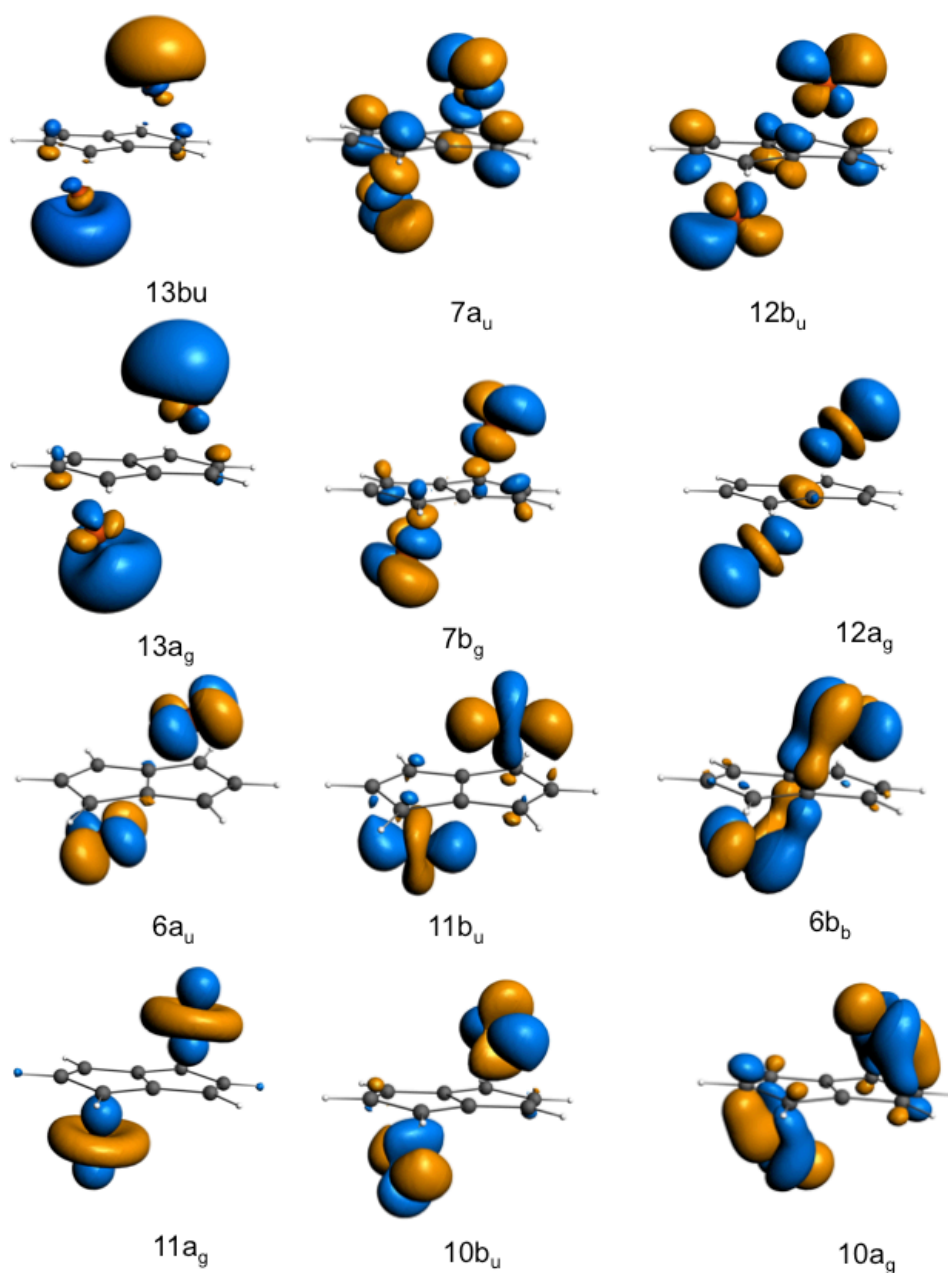


Fig. 16. Frontier orbitals of a M_2Pn fragment. The higher lying orbitals 13b_u-12a_g provide six orbitals that are available for bonding further ligands, the lower energy orbitals 6a_u to 10a_g correspond to t_{2g} sets of orbitals on each metal. They house 12 metal d electrons and may be employed in back-bonding to further ligands.[10]

The 7a_u and 12b_u orbitals are antibonding to the pentalene π_5 and π_4 pentalene orbitals respectively.

Extended Hückel calculations have been carried out on *anti*-Pn(FeCp)₂ as a model for *anti*-Pn(FeCp*)₂ which indicate the HOMO is an orbital of a_u symmetry.[72, 81] On oxidation to the mono-cation the unpaired electron occupies this orbital (Fig. 17). Further oxidation to the dication involves removal of a further electron from an orbital of b_g symmetry creating a triplet ground state. [*anti*-Fe₂PnCp*₂]⁺ shows a strong low energy absorption at 2200 nm[73] which is commonly described as an intervalent transition. However on a delocalised model it corresponds to an excitation of a β electron from the b_g or other metal orbital to the half-filled a_u orbital.

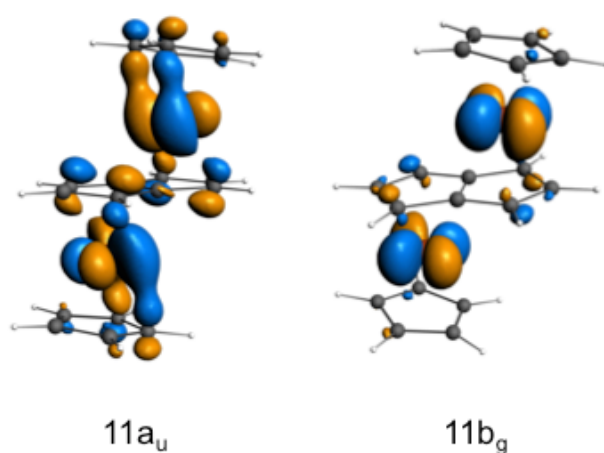


Fig. 17. Isosurfaces for the 11a_u and 11b_g orbitals of Fe₂PnCp₂ⁿ⁺. [10]

Co₂PnCp₂ is diamagnetic and has a HOMO of a_g symmetry as is Ni₂PnCp₂ with a HOMO of b_g symmetry (Fig. 17). Both these HOMOs are metal-pentalene antibonding, the Ni one more so than the Co one, and are the cause of the slippage of the metal away from the bridgehead carbons.

Calculations on *anti*- and *syn*-M₂Pn(CO)₆ (M=Mn and Re) indicate that for Re the isomers are almost isoenergetic whereas for Mn the anti-isomer is more stable by 24 kJ·mol⁻¹. [3] This is in agreement with the fact that both isomers are formed for Re but only the anti-isomer for Mn. [66]

5.3.2 *syn*-bimetallic complexes

When both metals are on the same side of the pentalene ligand there is the possibility of direct interaction between them. Whether this is bonding, non-bonding or antibonding has been a question of interest.

DFT calculations on *syn*-V₂Pn₂Cp₂ suggest the singlet ground state molecule has a triple bond of $\sigma^2\pi^2\delta^2$ configuration[64] (Fig. 18). The calculated V–V distance of 2.37 Å is in reasonable agreement with the value 2.5380(5) Å determined by X-ray diffraction studies. Magnetic measurements indicate a triplet excited state corresponding to occupation of a low lying δ^* orbital.[64] NMR spectroscopic and magnetic measurements place the excited state 14–17 kJ·mol⁻¹ above the singlet; however DFT calculations estimate the triplet state to be 30 kJ·mol⁻¹ more stable than the singlet.

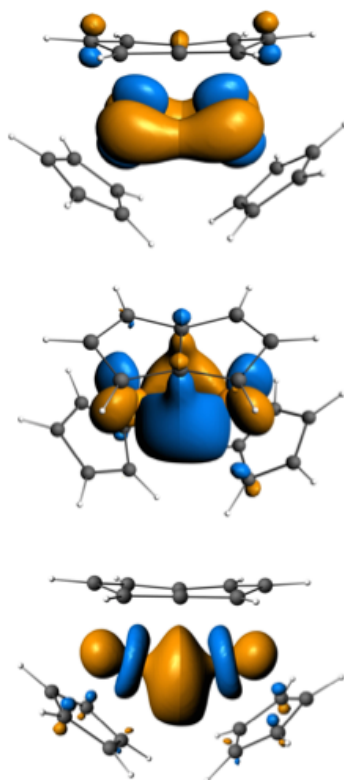


Fig. 18. Isosurfaces for the σ , π and δ V–V bonding orbitals of V₂PnCp₂. [10]

syn-Re₂Pn(CO)₆ has along Re–Re distance of 3.2329(3) Å and a non-planar pentalene system bent away from the metal centres indicative of steric repulsion between the Re(CO)₃ units.[66] *syn*-Fe₂Pn*(CO)₅ and *syn*-Co₂Pn*(CO)₄ are both synthesised from carbonyl dimers. Fragment analysis indicates an Fe–Fe antibonding interaction for the iron compound and a non-bonding one in the cobalt case.[70] The metal-metal distances (Fe1–Fe2 2.6869(5) Å and Co1–Co2 2.675(3) Å) are within the bonding range, but are constrained by the interaction with the bridging ligands. Fe₂Pn*(CO)₅ has an interesting structure in that the molecule has *C_s* rather than *C_{2v}* symmetry, with the bridging carbonyl lying to

one side of the plane passing through the Fe and wingtip C atoms. The HOMO, which back donates to the bridging carbonyl has a node in this plane so overlap is achieved by asymmetric placement of the ligand (Fig. 19).

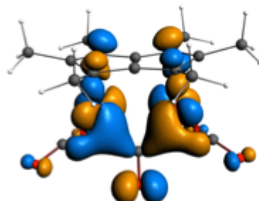


Fig. 19. Isosurface for the HOMO of $\text{Fe}_2\text{Pn}^*(\text{CO})_5$ showing back donation to the bridging carbonyl ligand.[10]

Group 9 bimetallic carbonyl complexes have been synthesised with the Pn^* ligand,[70, 76] and have the expected stoichiometry $\text{M}_2\text{Pn}^*_2(\text{CO})_4$. DFT calculations indicate that the *syn*-isomer is more stable than the *anti*-isomer, for $\text{M}=\text{Co}$ marginally so, with an increasing energy preference down the group, 8 $\text{kJ}\cdot\text{mol}^{-1}$ for Co, 30.5 $\text{kJ}\cdot\text{mol}^{-1}$ for Rh and 40.8 $\text{kJ}\cdot\text{mol}^{-1}$ for Ir. The *anti*-isomers have not been synthesised. The M–M bond orders are calculated as –0.11 for Co, –0.06 for Rh and 0.16 for Ir, thus no direct two electron M–M bond is indicated. The M–M distances of 2.675(3) Å for Co, 2.913(6) Å for Rh and 2.932(4) Å for Ir in the solid state structures also indicate the absence of a bond. Furthermore, the C5 rings of the pentalene ligand deviate in planarity in a direction *away* from the metals, as quantified by the relatively large hinge angles (Co 6.8°, Rh 11.4°, Ir 10.9°). The HOMO-1 for Co and the HOMO for Rh and Ir shows an antibonding interaction between the metals and the pentalene π_4 orbital but its effect is reduced by back donation to the carbonyls (Fig. 20), hence the shift of the metals away from the bridgehead carbons is small.

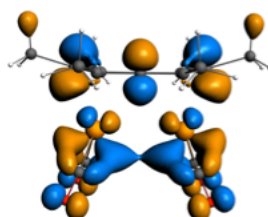


Fig. 20. HOMO for $\text{Rh}_2\text{Pn}^*(\text{CO})_4$ (the Ir analogue has a similar HOMO and the Co analogue a similar HOMO-1).[10]

6. Other bonding modes

A number of compounds have been synthesised where pentalene binds to a single metal in an η^5 mode. As pointed out by Saillard *et al.*, this tends to happen when the total electron count is greater than 18.[3]

Initial attempts by Katz and co-workers to prepare an iron pentalenide species resulted in dimerisation of the ligand and formation of a monometallic complex with a single C–C bond between pentalene ligands.[54] When 5 electrons are donated by one of the pentalene rings the other ring acquires an allyl like function. DFT studies show that the optimised SOMO of PnFeCp is primarily localised on C4 and C6 of the uncoordinated ring.(Fig. 21).[3]

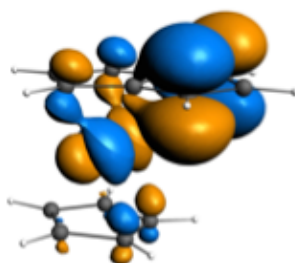


Fig. 21. Isosurface for the SOMO of PnFeCp . [3, 10]

With two pentalene ligands present the allyl radicals couple forming a *trans*-annular C–C bond; DFT calculations indicate a double C=C bond in the uncoordinated ring (Fig. 22).[10]

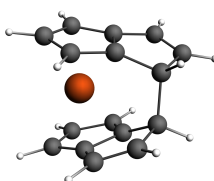
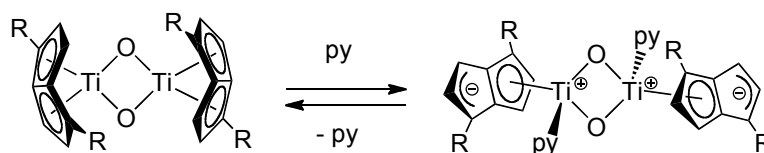


Fig. 22. Calculated structure of Pn_2Fe . [10]

Complexes of hydropentalene, such as $(\text{PnH})_2\text{Fe}$, [82] resemble cyclopentadienyl compound in their bonding and should possess a C=C double bond on the uncoordinated ring. However disorder in the crystal prevents unequivocal authentication of the C–C bond lengths.[83] Lithiation yields the dianion, $[\text{Pn}_2\text{Fe}]^{2-}$ which proves a useful synthon for further metallation, see Section 9 below.

Reactions causing a decrease in pentalene hapticity are known, for example a recent report by Kilpatrick and Cloke of a titanium oxo-bridged dimer in which the Pn^+ ligand changes hapticity from η^8 - to η^5 - mode upon addition of pyridine.[43] This results in a double zwitterionic structure, with a formal positive charge on each Ti(IV) centre and a negative charge on the noncoordinated part of the pentalene ligand.



Scheme 5. Change in hapticity of titanium oxo-bridged dimer upon reaction with pyridine. $\text{R} = \text{Si}^i\text{Pr}_3$. [43]

This unusual binding mode has previously been observed by Jonas and co-workers in the mononuclear complexes $(\eta^5\text{-Pn})\text{MCp}^*$ ($\text{M} = \text{Cr}, \text{Co}$ and Rh), and $\text{Li}_2[\text{Zr}(\eta^5\text{-Pn})\text{Me}_2]$ (Fig. 23). [84-86]

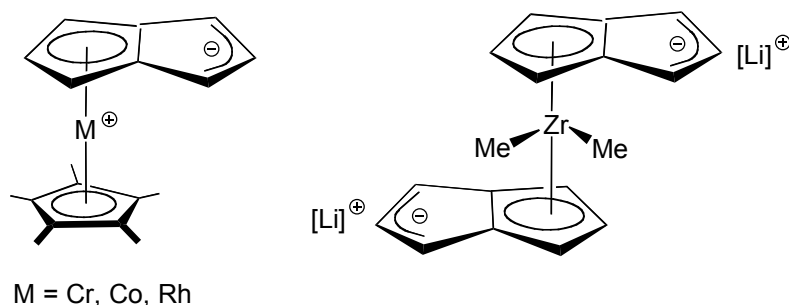


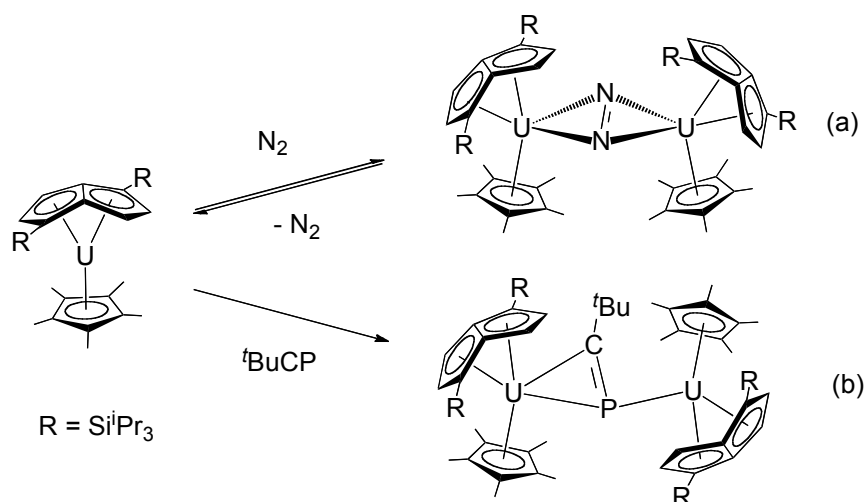
Fig. 23. Examples of mononuclear η^5 -pentalene complexes. [84-86]

7. Small molecule activation

In light of global energy demands there is considerable interest in the activation of small molecules (such as CO , CO_2 , N_2 , H_2 and CH_4) for use as chemical feedstocks for industrially important commodity chemicals. [87-89] The difficulty in achieving such transformations of small molecules often lies in the kinetic barrier to their activation, and as a result highly reducing metal complexes are typically employed. Pentalene ligands have shown the ability to stabilise complexes containing highly reactive metal centres, particularly when coordinated in an η^8 -mode to a early transition or f-block metal as previously described. [1] However, reports of small molecule activation in organometallic chemistry of pentalene are limited to a handful of examples.

Cloke and co-workers have reported the reaction of uranium(III) mixed-sandwich complex $(\eta^8\text{-Pn}^+)\text{UCp}^*$ with dinitrogen.[50] The reaction is reversible and the di-uranium(IV) product, $[(\eta^8\text{-Pn}^+)\text{UCp}^*]_2(\mu\text{-}\eta^2\text{:}\eta^2\text{-N}_2)$, features a 'side-on' bridging N_2 ligand in its molecular structure (Scheme 6). The N–N distance of 1.232(10) Å in this complex is lengthened with respect to free N_2 (1.098 Å)[90] indicating a significant activation resulting in a reduced formal bond order of two, which was supported by a DFT study.[91]

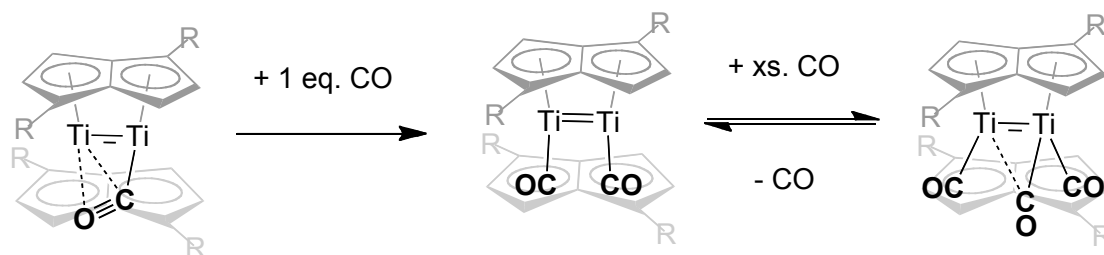
Another example of the reductive capability of $(\eta^8\text{-Pn}^+)\text{UCp}^*$ is found in the recent report of its reaction with the phosphalkyne, $^t\text{BuCP}$.[92] The solid state structure of the product isolated from this reaction, $[(\eta^8\text{-Pn}^+)\text{UCp}^*]_2(\mu\text{-}\eta^2\text{:}\eta^1\text{-}^t\text{BuCP})$, shows a $^t\text{BuCP}$ ligand which has been doubly reduced and binds to one of the U(IV) centres in an unprecedented η^2 -mode (Scheme 6).



Scheme 6. Activation of N_2 and $^t\text{BuCP}$ by a U(III) complex.[50, 92]

Cyclic voltammetry studies on $(\eta^8\text{-Pn}^+)\text{UCp}^*$ in $[\text{}^n\text{Bu}_4\text{N}][\text{B}(\text{C}_6\text{F}_5)_4]/\text{THF}$ suggest this uranium(III) pentalene complex is *ca.* 0.4 V more reducing than the analogous complex bearing the isoelectronic 1,4-bis(triisopropylsilyl)cyclooctatetraenyl $[\text{COT}^+]^{2-}$ ligand, $(\eta^8\text{-COT}^+)\text{UCp}^*\text{THF}$.[81] Furthermore the latter complex shows no reactivity with dinitrogen,[93] consistent with the additional electronic donation provided by the folded η^8 -carbocyclic ligand, Pn^+ , as compared with the planar COT^+ .

Group 4 metal pentalene complexes have shown fascinating reactivity. The di-titanium bis(pentalene) complex $\text{Ti}_2\text{Pn}^{\dagger}_2$ shows unprecedented reactivity amongst other known ‘double-sandwich’ complexes. The two pentalene ligands are bent around the Ti_2 core in the solid state structure, with an average centroid-metal-centroid angle of $155.2(2)^\circ$.^[47] This provides a relatively open structure in which the frontier orbitals are sterically accessible to small molecule substrates. The high energy electrons forming the $\text{Ti}=\text{Ti}$ double bond engage in donation and reduction. For example, reaction of $\text{Ti}_2\text{Pn}^{\dagger}_2$ with one or two equivalents of CO affords mono and di-carbonyl complexes respectively, which have been structurally characterised. Under excess of CO gas, a tri-carbonyl complex is formed, which has only been characterised *in situ* by low temperature NMR and IR spectroscopy (Scheme 7).



Scheme 7. Carbonyl complexes of $\text{Ti}_2\text{Pn}^{\dagger}_2$.^[40, 41, 43] R = Si^iPr_3 .

The monocarbonyl adduct has an unusual ‘side-on’ bound CO ligand rather than a symmetrical one. This was explained by DFT studies which show that the back donating orbitals from $\text{Pn}^{\dagger}_2\text{Ti}_2$ are of a_1 symmetry and would be orthogonal to the CO π^* orbitals if the CO were to be placed symmetrically. Back donation in all three carbonyls is shown in Fig. 23. Bonding between the Ti atoms is retained in all three cases.^[40]

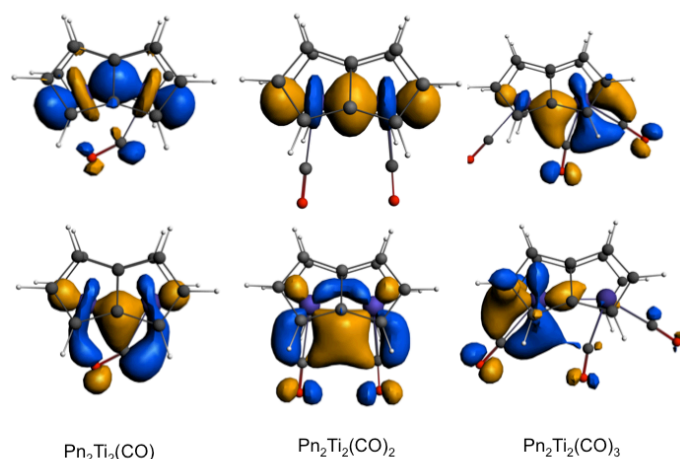
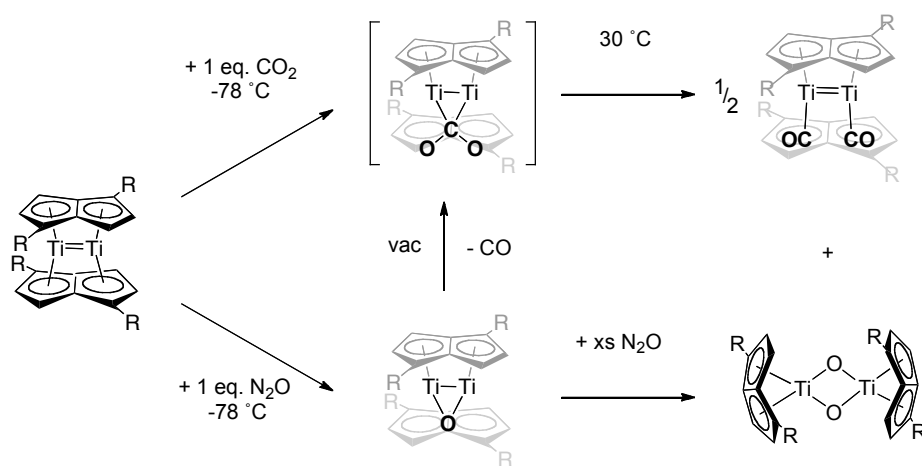


Fig. 24. Ti-Ti bonding orbitals and back-donation orbitals to the CO groups for $\text{Pn}_2\text{Ti}_2(\text{CO})_n$, $n = 1-3$. [40]

Reaction of $\text{Ti}_2\text{Pn}^{\dagger}_2$ with one equivalent of CO_2 at room temperature produces a 1:1 mixture of the dicarbonyl complex and a bis(oxo) bridged dimer $[(\eta^8\text{-Pn}^{\dagger})\text{Ti}(\mu\text{-O})]_2$. *In situ* NMR and IR spectroscopic studies revealed that a CO_2 adduct is formed with $\text{Ti}_2\text{Pn}^{\dagger}_2$ at low temperatures, which reacts further upon warming to RT. Exposure of $\text{Ti}_2\text{Pn}^{\dagger}_2(\text{CO}_2)$ to dynamic vacuum removes CO to form a diamagnetic mono(oxo) complex $\text{Ti}_2\text{Pn}^{\dagger}_2(\mu\text{-O})$, which was independently synthesised by reaction of $\text{Ti}_2\text{Pn}^{\dagger}_2$ with one equivalent of N_2O .



Scheme 8. Activation of CO_2 and N_2O by di-titanium bis(pentalene). $\text{R} = \text{Si}^i\text{Pr}_3$. [41]

The reaction pathway for the deoxygenation of CO_2 was modelled by DFT using two different methods (ADF:BP/TZP; Gaussian:B3LYP/SDD)(Fig.24). The transition state for rupture of a CO bond provided a good estimate of the experimental activation energy (Fig. 25). [41]

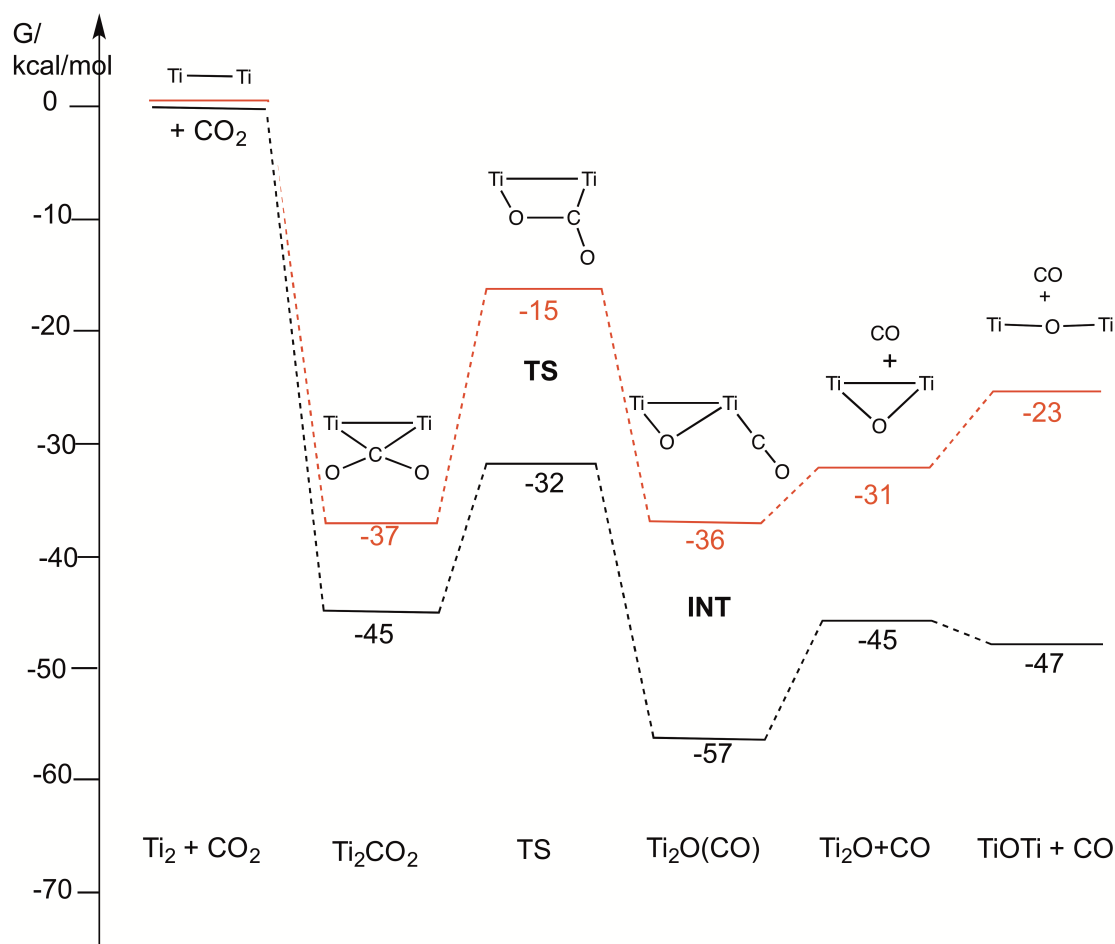


Fig. 25. Free energies for binding of CO₂ to Pn₂Ti₂ and the decomposition of Pn₂Ti₂(CO₂) under dynamic vacuum. ADF (BP/TZP) values are given in red and Gaussian (B3LYP/SDD) values in black. Adapted from [41].

The CO₂ adduct was calculated to have a symmetric structure with one of the Ti–Ti bonding orbitals donating into the bent LUMO of CO₂ (Fig. 26).[40] The other Ti–Ti bond was unperturbed.

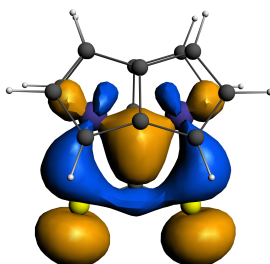


Fig. 26. The bonding orbital resulting from nucleophilic attack by Ti₂Pn₂ on CO₂. [40]

The thermally unstable CO₂ adduct was modeled by reactions of Ti₂Pn⁺₂ with its sulfur congener, CS₂[41] and heteroallenes such as *p*-tolylcarbodiimide.[38, 44] In these cases X-ray crystallography confirmed symmetrical binding of the

heteroallene molecule between the two Ti centres, acting a μ -Z type ligand in a neutral counting scheme (Fig. 27).

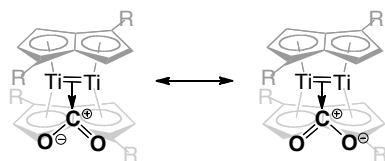
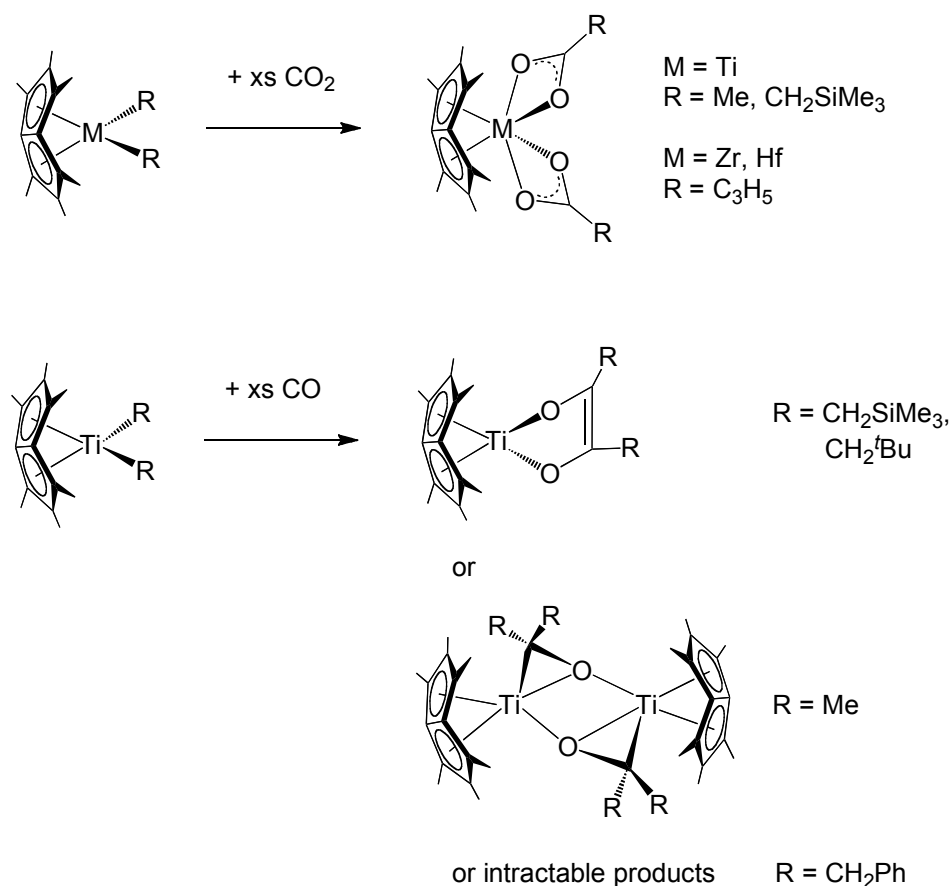


Fig. 27. Structure-bonding representation of CO_2 binding in μ -Z fashion to $\text{Ti}_2\text{Pn}^\dagger_2$. $\text{R} = \text{Si}^i\text{Pr}_3$. [40, 94]

The only other significant contribution to small molecule activation chemistry provided by organometallic pentalene complexes comes from recent reports of the permethylpentalene group(IV) metal hydrocarbyl complexes, $(\eta^8\text{-Pn}^*)\text{TiR}_2$; $\text{R} = \text{Me}$, CH_2Ph and $(\eta^8\text{-Pn}^*)\text{M}(\eta^3\text{-C}_3\text{H}_5)_2$; $\text{M} = \text{Zr}$, Hf and investigations into their reactions with CO_2 . [18, 42] These di-alkyl and bis-allyl complexes are 14 VE and 16 VE respectively, and both undergo insertion reactions with CO_2 into the $\text{M}-\text{C}$ bond, to yield di-carboxylate complexes, $(\eta^8\text{-Pn}^*)\text{M}(\kappa^2\text{-O}_2\text{CR})_2$ which are 18 VE (Scheme 9, top). These complexes have been structurally characterised for $\text{R} = \text{Me}$, CH_2Ph and each show symmetrical bidentate coordination of the RCO_2 units. [18, 42]

More interestingly, reactions of these complexes with CO led to direct reductive coupling of CO to give the mono cis-enediolate products, and a rare example of a dimeric titanaoxirane (Scheme 9, bottom).



Scheme 9. Activation of CO_2 [18, 42] and CO [95] by permethylpentalene group(IV) metal hydrocarbyl complexes.

8. Catalysis

In over 30 years since Sinn and Kaminsky's discovery that partially hydrolysed AlMe_3 , now known as methylaluminoxane (MAO), dramatically improves the activity of group 4 metallocenes for the polymerisation of ethylene and α -olefins,[96, 97] transition metal catalysts bearing cyclopentadienyl ligands have become ubiquitous in homogeneous Ziegler-Natta catalysis research.[98-101] In light of the intense exploration and commercialisation of new technologies based on single-site olefin polymerisation catalysts and the focus on the design of catalyst precursors, it seems surprising that there are very few catalytic applications of organometallic complexes with pentalene ligands reported in the literature.

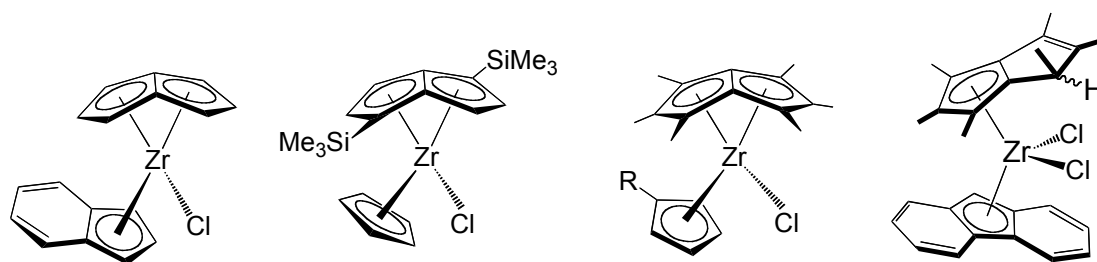


Fig. 28. Examples of group 4 pentalene complexes tested for olefin polymerisation activity.

Jonas and co-workers reported in the patent literature the ethylene polymerisation activity of $(\eta^8\text{-Pn})\text{-ZrCl}_2$, $(\eta^8\text{-Pn})\text{Zr(allyl)}_2$ and $(\eta^8\text{-Pn})\text{Zr(Ind)Cl}$, [39] and the latter was found to give the best activity of $712.0 \text{ kg}_{\text{PE}} \cdot \text{mol}^{-1} \cdot \text{h}^{-1} \cdot \text{bar}^{-1}$, which is rated as 'high' on the Gibson scale. [102] Cloke and co-workers have also reported patents for the synthesis of group 4 analogues with silylated pentalene ligands, $(\eta^8\text{-Pn}[1,4\text{-SiMe}_3]_2)\text{MCpCl}$ for $\text{M} = \text{Ti}, \text{Zr}$, and $(\eta^8\text{-Pn}[1,4\text{-SiMe}_3]_2)\text{ZrCp}^*\text{Cl}$, and their capacity to polymerise ethylene in the presence of MAO. [103] However, initial catalytic screenings did not show promising results and were not subsequently optimised.

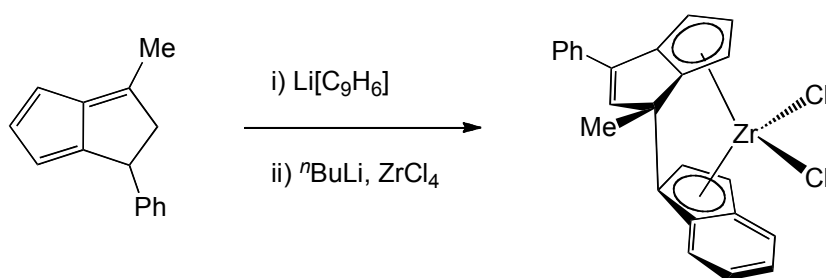
O'Hare and co-workers have tested the aforementioned titanium(IV) permethylpentalene di-alkyl complexes, $(\eta^8\text{-Pn}^*)\text{TiR}_2$ ($\text{R} = \text{Me}, \text{CH}_2\text{Ph}, \text{CH}_2\text{SiMe}_3$ and CH_2^tBu), [95] for the homogeneous polymerisation of ethylene in combination with borane and borate activators. [104] Despite the electron deficiency of these 14 VE complexes, the best complex ($\text{R} = \text{CH}_2\text{SiMe}_3$) showed moderate activity on the Gibson scale, [102] with co-catalyst $[\text{Ph}_3\text{C}][\text{B}(\text{C}_6\text{F}_5)_4]$. Recently these researchers have reported the synthesis and characterisation of a series of 18 VE group 4 mixed-ring complexes, $(\eta^8\text{-Pn}^*)\text{MCp}_{2-x}\text{Cl}_x$, ($\text{M} = \text{Ti}, \text{Zr}, \text{Hf}$; $x = 0, 1$), [14] and $\text{Pn}^*\text{MCp}^{\text{R}}\text{X}$ ($\text{M} = \text{Ti}, \text{Zr}$; $\text{Cp}^{\text{R}} = \text{Cp}, \text{Cp}^{\text{Me}}, \text{Cp}^t\text{Bu}, \text{Cp}^n\text{Bu}, \text{Cp}^{\text{Me}_3}, \text{Ind}$; $\text{X} = \text{Cl}, \text{Me}$), [45] which are more promising precatalysts for the homogeneous polymerisation of ethylene. The zirconium complexes in the presence of MAO showed very high activity on the Gibson scale, [102] with most complexes 2 orders of magnitude more active than their titanium analogues. The best performing homogeneous catalyst was $\text{Pn}^*\text{Zr(Ind)Cl}$ with an activity of $3585 \text{ kg}_{\text{PE}} \cdot \text{mol}^{-1} \cdot \text{h}^{-1} \cdot \text{bar}^{-1}$ recorded at modest $[\text{Zr}]:[\text{Al}]$ ratios of 1:250. [45] The very high activities shown by these electronically saturated (18 VE) catalysts poses an

interesting challenge in terms of mechanistic rationale; the traditional polymerisation mechanism for 16 VE Cp_2MCl_2 complexes that proceeds *via* the 14 VE alkyl cation $[\text{Cp}_2\text{MR}]^+$ does not appear to be accessible for the $\text{Pn}^*\text{MCp}^{\text{RX}}$ system.

The $\text{Pn}^*\text{MCp}^{\text{RX}}$ complexes were also immobilised on solid supports, including on a MAO-modified silica (ssMAO), a MAO-modified layered double hydroxide (LDH-MAO) and an insoluble polymethylaluminoxane (sMAO), for further study as slurry polymerisation catalysts. Remarkably, the catalysts supported on sMAO showed enhanced performance compared to the equivalent precatalysts in the solution phase, up to a maximum activity of $4486 \text{ kg}_{\text{PE}} \cdot \text{mol}^{-1} \cdot \text{h}^{-1} \cdot \text{bar}^{-1}$. Furthermore, the polyethylene produced by these slurry-phase systems displayed improved physical properties compared to their homogenous counterparts, such as a reduction in particle aggregation.

Half-sandwich zirconium complexes based on the (hydro)permethylpentalene ligand, $[\text{Pn}^*(\text{H})\text{ZrCl}_3]_2$, $\text{Pn}^*(\text{H})\text{Zr}[\text{NP}(\text{NMe}_2)_3]\text{Cl}_2$ and $\text{Pn}^*(\text{H})(\text{Flu})\text{ZrCl}_2$, immobilised on a LDH-MAO support, have also been studied for slurry-phase ethylene polymerisation. The (hydro)permethylpentalenyl complex, $[\text{Pn}^*(\text{H})\text{ZrCl}_3]_2$, polymerises ethylene four times faster than the non-hydrogenated, $[\text{Pn}^*\text{Zr}(\mu\text{-Cl})_{3/2}]_2\text{Li} \cdot \text{THF}_x$ under similar experimental conditions, with an activities of 89 and $24 \text{ kg}_{\text{PE}} \cdot \text{mol}^{-1} \cdot \text{h}^{-1} \cdot \text{bar}^{-1}$ respectively. [105]

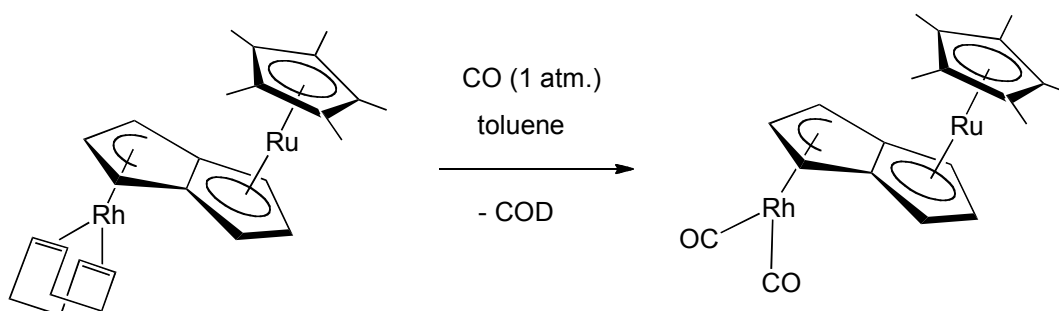
The use of pentalenes in *ansa*-metallocenes has been limited, presumably due to the limited availability of a suitable tethered ligand precursor. Erker and co-workers have reported unsymmetrically bridged *ansa*-zirconocene complexes bearing novel 3-dimethylamino-1,2-dihydropentalene derived ligand systems.[106] An example of a mixed pentalene-indenyl *ansa*-metallocene has also been reported, which was synthesised by reaction of a di-substituted hydropentalene with an indenyl salt to form the annulated ligand *in situ* followed by reaction with ZrCl_4 (Scheme 10).[107] This bridged zirconocene has been used in the co-polymerisation of ethylene with cyclic olefins.[108]



Scheme 10. Synthesis of an *ansa*-zirconocene from dihydropentalenes.[107]

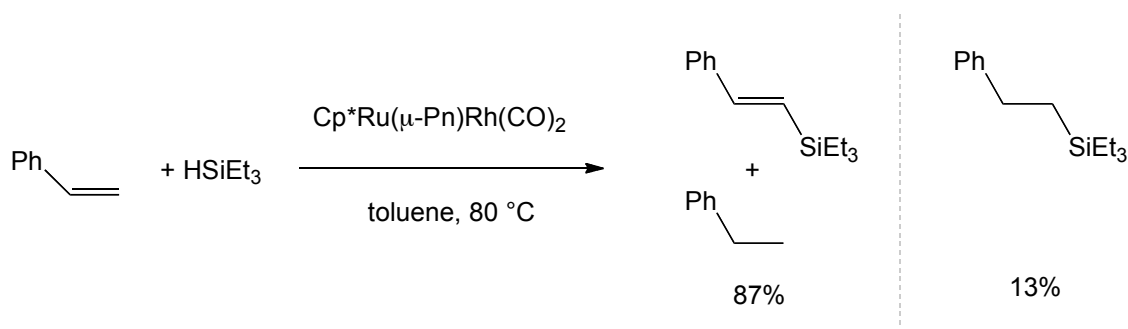
Outside the field of olefin polymerisation, reports of pentalene complexes with catalytic behavior in the literature are limited to two examples.

In 2001 Manriquez and co-workers reported an asymmetric heterobimetallic complex, $\text{Cp}^*\text{Ru}(\mu\text{-}\eta^5\text{:}\eta^3\text{-Pn})\text{-Rh}(\eta^4\text{-COD})$ (COD = 1,5-cyclooctadiene), synthesised *via* a stepwise 'building block' method from $[\text{Cp}^*\text{Ru}(\eta^5\text{-Pn})]$ [Li] and $[\text{Rh}(\eta^4\text{-COD})\text{Cl}]_2$ (Scheme 11).[109, 110]



Scheme 11. Synthesis of $\text{Cp}^*\text{Ru}(\mu\text{-}\eta^5\text{:}\eta^3\text{-Pn})\text{Rh}(\text{CO})_3$. [109]

$\text{Cp}^*\text{Ru}(\mu\text{-}\eta^5\text{:}\eta^3\text{-Pn})\text{Rh}(\eta^4\text{-COD})$ reacts with carbon monoxide, displacing the COD ligand to afford $\text{Cp}^*\text{Ru}(\mu\text{-}\eta^5\text{:}\eta^3\text{-Pn})\text{Rh}(\text{CO})_3$ (Scheme 12), which is a relatively unstable species and was characterised solely by IR and NMR spectroscopic methods. This complex is of interest in the context of cooperative interactions between metals, which are known to enhance reactivity in small molecule activation,[111-115] and improve the rate of certain catalytic processes.[116-118] Indeed, $\text{Cp}^*\text{Ru}(\mu\text{-}\eta^5\text{:}\eta^3\text{-Pn})\text{-Rh}(\text{CO})_3$ shows one of the highest activities as a precatalyst for the dehydrogenative silylation of styrene (Scheme 12).



Scheme 12. Catalytic dehydrogenative silylation of styrene by a Ru/Rh complex.[109]

In 2014, Turner *et al.* reported a series of group 4 alkoxide and aryloxy complexes with a (hydro)permethylpentalene ligand, $\text{Pn}^*(\text{H})\text{MCl}_3\text{-}_x(\text{OR})_x$; $\text{M} = \text{Ti}$: $x = 3$, $\text{R} = ^t\text{Bu}$, 2,6-Me- C_6H_3 , $S\text{-CH}[\text{CH}_3]\text{C}_6\text{H}_5$. $\text{M} = \text{Zr}$: $x = 3$, $\text{R} = ^t\text{Bu}$, OCH_2Ph , $S\text{-OCH}[\text{CH}_3]\text{C}_6\text{H}_5$, *rac*- $\text{OCH}[\text{CH}_3]\text{C}_6\text{H}_5$, 2,6-Me- C_6H_3 , 2,6-*i*Pr- C_6H_3 ; $x = 1$, 2,6-*t*Bu- C_6H_3 . $\text{M} = \text{Hf}$: $x = 3$, $\text{R} = 2,6\text{-Me-C}_6\text{H}_3$; $x = 2$, $\text{R} = 2,6\text{-}^i\text{Pr-C}_6\text{H}_3$; $x = 1$, 2,6-*t*Bu- C_6H_3 . [119] In each case the methyl group attached to the sp^3 -hybridised carbon atom of $\text{Pn}^*(\text{H})$ was assigned to an *anti* configuration with respect to the metal cation, and present in a mixture of two diastereomers (R,R_P) - and (S,S_P) - $\text{Pn}^*(\text{H})\text{M}(\text{OR})_3$ (outlined in red in Fig. 29); the R,S_P and S,R_P analogues were not observed.

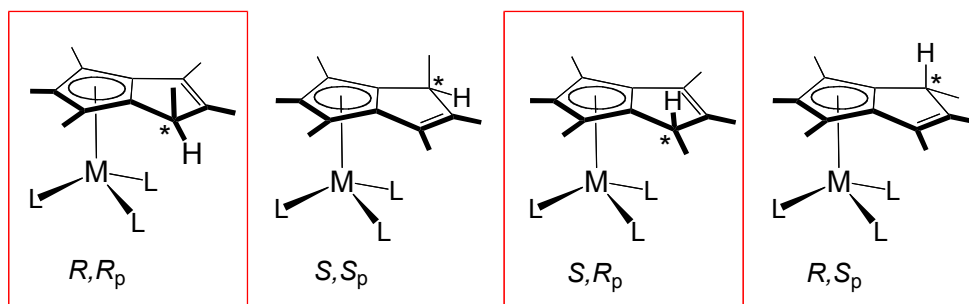
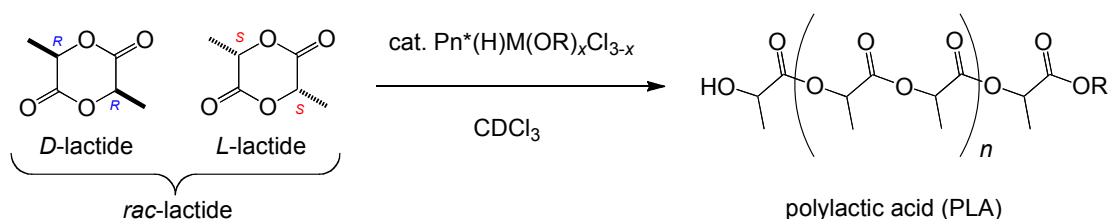


Fig. 29. Possible diastereomers of $\text{Pn}^*(\text{H})\text{ML}_3$ for non-chiral L.

The complexes were investigated as initiators for the ring-opening polymerisation of polar monomers (L- and *rac*-lactide) in order to ascertain if these mixtures of diastereomers could exert any stereocontrol on the resulting polymerisation.

All complexes in the series were shown to be good initiators for lactide polymerisation, with the rate of initiation following a general trend of $[\text{Zr}] > [\text{Hf}] > [\text{Ti}]$. The benzyl alkoxide derived complexes $\text{Pn}^*(\text{H})\text{Zr}(S\text{-OCH}[\text{CH}_3]\text{C}_6\text{H}_5)_3$ and $\text{Pn}^*(\text{H})\text{Zr}(\text{rac-OCH}[\text{CH}_3]\text{C}_6\text{H}_5)_3$ demonstrated rates of polymerisation

comparable to those of many of the fastest initiators in the literature, with low polydispersities (1.14–1.15) suggesting a controlled polymerisation process (Scheme 13).



Scheme 13. Ring-opening polymerisation of lactide monomers by chiral $\text{Pn}^*(\text{H})$ group 4 metal alkoxide/aryloxide complexes.

It was intended that the $\text{Pn}^*(\text{H})$ ligand, which can be viewed as a chiral Cp' ligand in these half-sandwich complexes, would impart stereocontrol on the polylactide resin produced. However, only atactic polymers were obtained from the polymerisation of *rac*-lactide and no epimerisation was observed in the polymerisation of *L*-lactide. It was proposed that the chiral centre of the $\text{Pn}^*(\text{H})$ ligand is too remote from the metal centre, and the methyl substituents too small to exert any stereochemical effect.

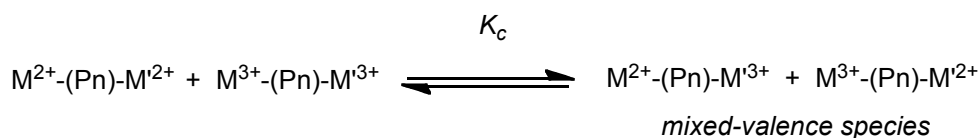
9. Intermetallic communication

Molecules containing more than one metal centre can exhibit profoundly different physical properties and reactivity to monometallic complexes, particularly where there is a strong interaction between the metal centres.[120] The synthesis of polymers that contain metallocene units in close proximity are highly desirable as they should allow extended metal–metal interactions throughout the chain. In such cases, polymers with interesting electrical, magnetic or other physical properties might be envisaged.[121] A brief overview of the classification of the mixed-valence (MV) state with a particular focus on pentalene bridged bimetallics is presented herein.

In a complex with two redox centres that are electronically coupled to some extent, e.g. a generic pentalene bridged bimetallic $\text{L}_n\text{M}(\mu\text{-Pn})\text{M}'\text{L}_n$ (where M and M' are divalent in the reduced form), removal of an electron creates a so-called MV system, with two formally different oxidation states. Depending on the strength of the electronic coupling, the unpaired electron is either concentrated

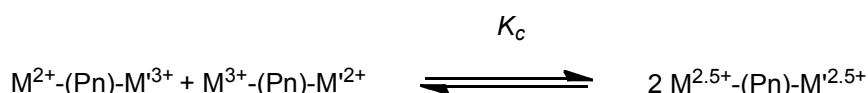
on one of the redox centres, or it is symmetrically delocalised between the two sites. These are the extreme situations (I and III respectively) of the Robin-Day classification for a MV species.[122, 123] Class I bimetallic compounds show no metal-metal interactions and have electronic properties corresponding to the separate sites M^{n+} and $M^{(n+1)+}$, Class III systems have very strong metal-metal interactions and are obvious candidates for use as ‘molecular wires’ in the field of molecular electronics.[124] Between these two extremes are Class II complexes, which exhibit intermediate metal-metal interactions. Where a bimetallic complex lies in this classification depends on the strength of electronic coupling, and can be investigated using a number of physical techniques.

Electrochemical methods, particularly cyclic voltammetry (CV), provide a convenient way of inferring the extent of delocalisation in MV state. In the case of a homo-bimetallic compound ($M = M'$) two redox processes ($E^{(1)}$ and $E^{(2)}$) should be observed. The potential difference between two *reversible* electrochemical processes, $\Delta E_{1/2} = |E_{1/2}^{(1)} - E_{1/2}^{(2)}|$, is indicative of the thermodynamic stability of the MV state with respect to other redox states. $\Delta E_{1/2}$ separations close to zero are characteristic of non-interacting metal sites (Class I), either due to large distance between them or because the ligand does not provide an electronic coupling pathway. Small values of $\Delta E_{1/2}$ suggest weak electronic coupling, corresponding to a small comproportionation constant K_c (Scheme 14) and a MV state involving so-called ‘trapped’ valence metal centres (Class II).



Scheme 14. Formation of Class I and II mixed-valence pentalene bridged bimetallics, where K_c = comproportionation equilibrium constant.

Large $\Delta E_{1/2}$ separations (above *ca.* 200 mV, corresponding to $K_c \geq 10^4$, Scheme 15) are commonly cited as evidence for a highly delocalised system with a strong degree of thermodynamic stabilisation of the MV state (Class III).



Scheme 15. Fully delocalised Class III bimetallics with large K_c .

In the case of heteronuclear complexes ($M \neq M'$) a non-zero $\Delta E_{1/2}$ is expected even in the absence of any metal-metal interactions, due to the different redox properties of metal centres present in the molecule.

Assigning Robin-Day classification to electronic interaction in a MV species should not be based on $\Delta E_{1/2}$ alone, since it is purely a measure of thermodynamic stabilisation of the MV state for which other energetic terms such as through-space electrostatics, solvation or entropy may also make a significant contribution.[125] However electrochemical methods such as CV are a useful screening technique for bimetallic complexes, which may exhibit other interesting interactions. For example MV species can exhibit strong intervalence charge transfer (IVCT) bands in the near-infrared (NIR). Other techniques commonly used include EPR and ^{57}Fe Mössbauer spectroscopy to study the electronic and nuclear interactions respectively, SQUID magnetometry for magnetic interactions, and NMR spectroscopy and X-ray crystallography to provide structural information in the solution and solid state.

9.1 Electronic delocalisation in pentalene-bridged complexes

The aromatic nature of the pentalene ligand has been shown to induce very strong electronic delocalisation in anti-bimetallic complexes and promote coupling effects through the planar π -system. Metal-metal interactions have been studied extensively by Manriquez and co-workers for the capped triple decker-complexes $[\text{Cp}^*\text{M}(\mu\text{-}\eta^5\text{:}\eta^5\text{-Pn})\text{MCp}^*]^{n+}$ with transition metals (Fig. 29(a), $M = \text{Fe}, \text{Co}, \text{Ni}, \text{Ru}$) using a variety of physical techniques.[72, 73, 126, 127]

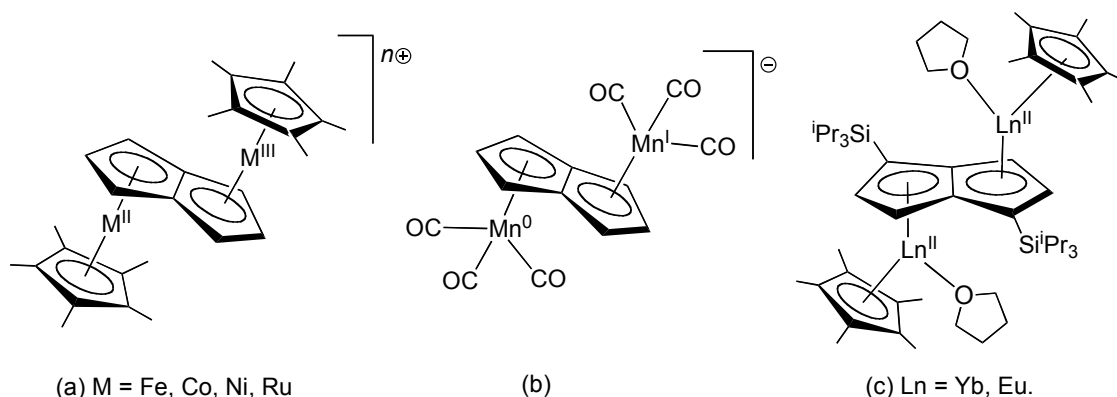


Fig. 30. Examples of anti-bimetallic complexes studied for metal-metal interactions.

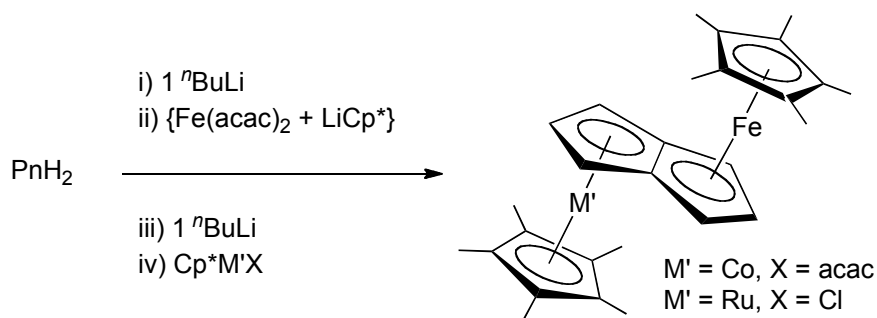
Cyclic voltammetry shows that these compounds undergo two successive one-electron transfers, with large potential separations between successive oxidations (decreasing in the order $\text{Fe} > \text{Co} > \text{Ni} > \text{Ru}$). Oxidation to the cationic forms ($n = +1$ and $+2$) was achieved for each complex, of which the MV forms ($n = +1$) show IVCT bands in the NIR spectrum that are not observed in the neutral or di-cationic forms. ^{57}Fe Mössbauer spectroscopy (timescale $\approx 10^{-7}$ s) studies of the cationic $[\text{Cp}^*\text{Fe}(\mu\text{-}\eta^5\text{:}\eta^5\text{-Pn})\text{FeCp}^*]^+$ species found the iron environment to be fully averaged down to 1.5 K, indicative of a strong electronic interaction between the metal centres and extensive delocalisation in the MV state.

Bimetallic complexes of group 7 metal carbonyls, $[\text{M}(\text{CO})_3]_2(\mu\text{:}\eta^5\text{:}\eta^5\text{-Pn})$ for $M = \text{Mn}$ and Re , were synthesised by treatment of $[\text{Li}(\text{DME})]_2\text{Pn}$ with two equivalents of $\text{Mn}(\text{CO})_3(\text{py})_2\text{Br}$ or one equivalent of $[\text{Re}(\text{CO})_3(\text{THF})\text{Br}]_2$ respectively.[66] The manganese(I) complex, formed as an exclusively *anti*-bimetallic, is particularly noteworthy. $[\text{Mn}(\text{CO})_3]_2(\mu\text{:}\eta^5\text{:}\eta^5\text{-Pn})$ may be reduced by electrochemical or chemical methods to yield both the dianion as a dilithium salt, or the mono-anion stabilised by a $[\text{FeCp}(\text{C}_6\text{Me}_6)]^+$ counterion (Fig. 29 (b)). The latter is formally a $\text{Mn}(\text{I})/\text{Mn}(\text{0})$ mixed-valence complex and shows hyperfine coupling with the two equivalent ^{55}Mn ($I = 5/2$) centres in the EPR spectrum, consistent with a Robin-Day class III system.[128] This MV anion remains one of the most delocalised organometallic systems reported to date.

Anti-bimetallic complexes of the divalent lanthanides with silylated pentalene ligands, $[\text{Cp}^*\text{Ln}(\text{THF})]_2(\mu\text{:}\eta^5\text{:}\eta^5\text{-Pn}^+)$ for $\text{Ln} = \text{Eu}$ and Yb (Fig. 29 (c)), were prepared from the one-pot reaction of $\text{LnI}_2(\text{THF})_x$ and KCp^* and the subsequent addition of half an equivalent of $[\text{K}]_2\text{Pn}^+$.[79] These complexes are of interest as

molecular models for lanthanide-based polymers, which have potential applications as magnetic materials,[129, 130] molecular catalysis,[131, 132] and luminescent devices.[133, 134] CV studies indicated that $[\text{Cp}^*\text{Eu}(\text{THF})]_2(\mu\text{:}\eta^5, \eta^5\text{-Pn}^+)$ decomposes readily upon oxidation but the $[[\text{Cp}^*\text{Yb}(\text{THF})]_2(\mu\text{:}\eta^5, \eta^5\text{-Pn}^+)]^+$ mono-cation appeared to be stable under the conditions and timescale of the experiment. Furthermore through-ligand Yb–Yb coupling was suggested by the electrochemical data for $[\text{Cp}^*\text{Yb}(\text{THF})]_2(\mu\text{:}\eta^5, \eta^5\text{-Pn}^+)$, of magnitude similar to that of its transition metal analogues.

Despite the number of pentalene-bridged homobimetallic compounds of the general formula $L_n\text{M}(\mu\text{-}\eta^5\text{:}\eta^5\text{-Pn})\text{M}'L_n'$ ($\text{M} = \text{M}'$) that have been synthesised, comparatively few heterobimetallic ($\text{M} \neq \text{M}'$) examples are known. The main synthetic challenge is selective coordination of two different metal centres to the pentalene bridge to give a mixed-metal complex, whilst preventing formation of homobimetallic species. Strategies for the rational synthesis of such materials were pioneered by Manriquez and co-workers starting with dihydropentalene *via* successive deprotonation and incorporation of the appropriate metal half-sandwich synthon (Scheme 16).[73]



Scheme 16. 'Building block' synthetic route to heterobimetallics.[73]

The heterobimetallic complex $[\text{Cp}^*\text{Ru}(\mu\text{-}\eta^5\text{:}\eta^5\text{-Pn})\text{FeCp}^*]^+$ was studied by ^{57}Fe Mössbauer spectroscopy, which indicates full delocalisation and a unique Fe environment for the mono-cation over the entire temperature range 1.5–300 K.[135, 136]

It has been suggested that the pentalene ligand allows an extent of electronic communication between the Fe/Ru centres that is not observed

between these metal centres with other unsaturated bridging ligands such as fulvalene.[136, 137] The MV form of both heteronuclear complexes $[\text{Cp}^*\text{M}'(\mu\text{-}\eta^5\text{:}\eta^5\text{-Pn})\text{FeCp}^*]^+$ $\text{M}' = \text{Ru}$ and Co , exhibit IVCT bands in the NIR region not observed in the neutral and di-cationic species, and were classified as Class III and Class II respectively.

In a modification of the 'building block' synthetic route, $\text{Fe}(\eta^5\text{-PnH})_2$ was lithiated *in situ* and used to incorporate a Cp^*Co unit into the chain, forming $\text{Cp}^*\text{Co}(\mu\text{-}\eta^5\text{:}\eta^5\text{-Pn})\text{Fe}(\eta^5\text{-PnH})$ (Fig. 30, left), classified as an *asymmetric* anti-bimetallic due to the different ligand environments of the two metals ($\text{L}_n \neq \text{L}_n'$). [126] Interestingly the introduction of asymmetry in the ligand environment in $[\text{Cp}^*\text{Co}(\mu\text{-}\eta^5\text{:}\eta^5\text{-Pn})\text{Fe}(\eta^5\text{-PnH})]^+$ leads to Class I behavior based on the electrochemical (CV) and spectroscopic (NIR, Mössbauer) evidence,[93] whereas the symmetric congener $[\text{Cp}^*\text{Co}(\mu\text{-}\eta^5\text{:}\eta^5\text{-Pn})\text{FeCp}^*]^+$ is Class II. It was suggested that ligand asymmetry in general introduces a barrier for electron transfer and as a result decreases the extent of electronic interaction. This has a larger impact for heteronuclear complexes which already have an built-in barrier for electron transfer from the different electronic nature of the metal centres, and the subtle effect of changing the terminal ligand in this case can cause a complete loss of electronic communication.

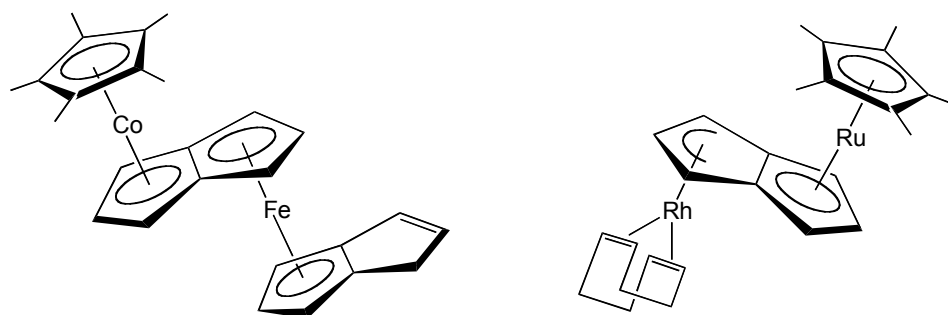
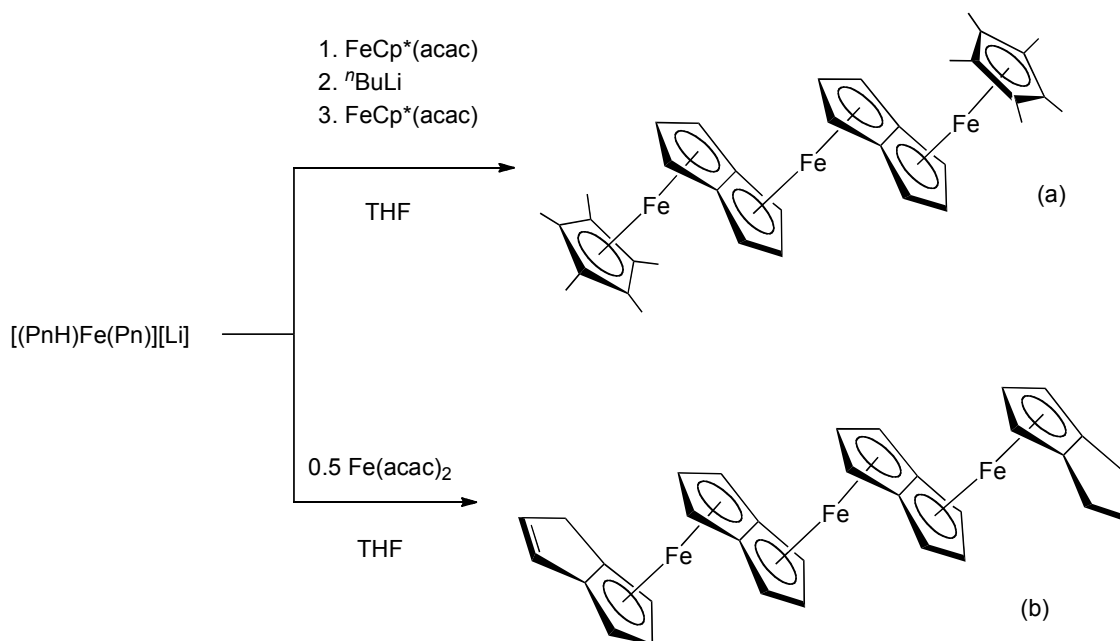


Fig. 31. Examples of hetero-bimetallics with asymmetric ligand environments.

The synthesis of oligomeric or polymeric materials consisting of alternating metal atoms and fused-ring ligands is expected to offer a range of interesting delocalised properties.[120] Theoretical studies by Matsuura *et al.* on 1D extended $[\text{Pn}(\text{M})]_n$ repeat units have predicted rich electronic properties,[138,

139] for example to $M=Fe$ 'nanowire' is predicted to show relatively large bandwidths as compared to other ferrocene polymers. Strategies for the rational synthesis of such materials were pioneered by Manriquez *et al.* who extended work on bimetallic pentalene systems described above to incorporate further organometallic fragments into the chain.[126]



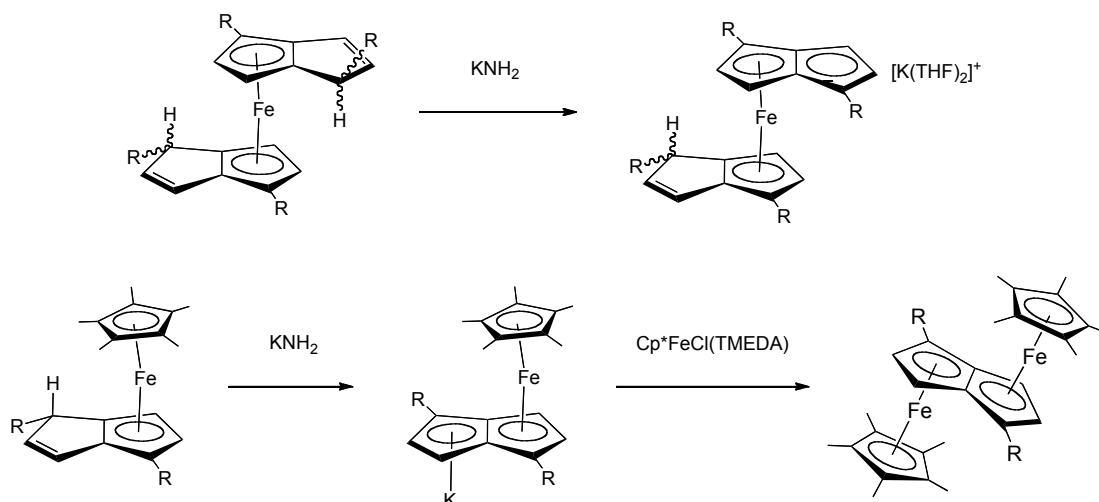
Scheme 17. Synthetic routes to trimetallic pentalene complexes.[126]

The fully capped trimetallic complex $(Cp^*Fe)_2[Pn_2Fe]$ was synthesised from $Fe(\eta^5-PnH)_2$ by lithiation with $nBuLi$ followed by addition of $FeCp^*(acac)$ in two successive iterations (Scheme 17 (a)). A potentially iterative process to higher chain oligomers was presented in the synthesis of a novel quadruple decker iron-pentalene complex from reaction of $[Li][PnFe(\eta^5-PnH)]$ with 0.5 equivalents of $Fe(acac)_2$ in THF (Scheme 17 (b)). The quadruple-decker complex $(\eta^5-PnHFe)_2[Pn_2Fe]$ was characterised by mass spectrometry and IR spectroscopy, however NMR and structural characterisation by single crystal X-ray diffraction were hampered by its low solubility in hydrocarbon solvents (400 mg L^{-1} of boiling toluene), and this has prevented synthesis of higher chain oligomers.

Subsequent investigations employing alkylated pentalene ligands, $C_8H_5(1-R)$ $R = Me, Et, iPr$, successfully introduced a greater degree of solubility in hydrocarbons

to the resulting iron(II) complexes.[140, 141] However, due to the lack of symmetry in these ligands, a mixture of isomeric multi-decker species were isolated as oils which could not be purified, and precluded full characterisation. The formation of multiple isomers also prevented unambiguous assignment of the electrochemical data obtained, and their potential as delocalised organometallic polymers could not be fully determined.

A range of iron(II) complexes incorporating the silylated pentalene ligands, $\text{Pn}^{\dagger}(\text{H})$ and Pn^{\dagger} , have recently been reported.[74] A combination of NMR spectroscopic and X-ray crystallographic methods were used to elucidate the two isomers that form in the case of the homoleptic complex $\text{Fe}(\eta^5\text{-Pn}^{\dagger}\text{H})_2$ (Scheme 18). Synthetic studies showed that $\text{Fe}(\eta^5\text{-Pn}^{\dagger}\text{H})_2$ could be singly deprotonated to form the mono-potassium salt $(\eta^5\text{-Pn}^{\dagger}\text{H})\text{Fe}[\eta^5\text{-Pn}^{\dagger}(\eta^5\text{-K}(\text{THF})_2)]$, however the latter was unsuitable as a synthon for incorporating further metal fragments into the chain, and instead underwent decomposition reactions to afford a mixture of isomers. The mixed sandwich complex $\text{Cp}^*\text{Fe}(\eta^5\text{-Pn}^{\dagger}\text{H})$ was isolated as a single isomer, and deprotonated to give a potassium salt, $[\text{Cp}^*\text{Fe}(\mu\text{-}\eta^5\text{:}\eta^5\text{-Pn}^{\dagger})][\text{K}]$. The latter complex presents a potentially useful precursor for other Fe/M anti-bimetallics or for introducing additional substituents to the Pn^{\dagger} ligand.



Scheme 18. Synthesis of homo and heterobimetallic complexes of iron(II) with silylated pentalene ligands. $\text{R} = \text{Si}^i\text{Pr}_3$. [74]

A salt metathesis reaction of $[\text{Cp}^*\text{Fe}(\mu\text{-}\eta^5\text{:}\eta^5\text{-Pn}^{\dagger})][\text{K}]$ with $\text{Cp}^*\text{FeCl}(\text{TMEDA})$ resulted in the homonuclear bimetallic $[\text{Cp}^*\text{Fe}]_2(\mu\text{-}\eta^5\text{:}\eta^5\text{-Pn}^{\dagger})$ (Scheme 16,

however, this synthetic route was unsuccessful for the synthesis of a heterobimetallic complex with lanthanide metals Yb and Sm. DFT studies on model mono-Fe complexes revealed that the uncoordinated C atoms of the pentalene ligand carry a net negative charge, and hence the observed reactivity was attributed to the steric bulk of the Si^iPr_3 substituents.

10. Conclusions

This review demonstrates the versatility of the pentalene ligand in its organometallic complexes, which display interesting electronic and magnetic properties and also show novel reactivity. The wide variety of coordination modes are well accounted for by theory, which gives a good account of observed structural features. Examination of the orbital structure enables establishment of guidelines for electron counting in pentalene complexes. Where pentalene stabilises low oxidation states in metal complexes, for example Ti(II) and U(III), reductive activation of small molecules is evident. Zirconium complexes with pentalene ligands have attracted growing interest the field of in catalytic olefin polymerisation, and have been developed into solid-supported catalysts producing polyethylene with industrial-grade physical properties. Group 4 (hydro)permethylpentalene complexes are also competent initiators for the ring opening-polymerisation of lactides, an area of great interest for the production of sustainable, biodegradable plastics. When acting as a bridging ligand between metals, pentalene enables strong electronic coupling but synthetic challenges have so far hindered extension of a metal chain beyond a few metal centres.

Acknowledgements

A.F.R.K thanks Wadham College Oxford for a non-stipendiary Junior Research Fellowship.

Abbreviations

BH	bridgehead
COT	C ₈ H ₈
COT [†]	C ₈ H ₆ (Si ⁱ Pr ₃ -1,4) ₂
Cp'	generic abbreviation for a cyclopentadienyl ligand
Cp	C ₅ H ₅
Cp*	C ₅ Me ₅
Ct	ring centroid
CV	cyclic voltammetry
DFT	density functional theory
FA	fold angle
Flu	fluorenyl, C ₁₃ H ₉
HA	hinge angle
HOMO	highest occupied molecular orbital
Ind	indenyl, C ₉ H ₇
IVCT	inter-valence charge transfer
Ln	lanthanide metal
MAO	methylaluminoxane
MO	molecular orbital
MV	mixed-valence
NIR	near infra-red
NWT	non-wingtip
Pn'	generic abbreviation for a pentalene ligand
Pn	C ₈ H ₆
Pn*	C ₈ Me ₆
Pn [†]	C ₈ H ₄ (Si ⁱ Pr ₃ -1,4) ₂
SOMO	singly occupied molecular orbital
TMEDA	<i>N,N,N',N'</i> -Tetramethylethylenediamine
Tp ^{Me2}	hydrotris(3,5-dimethylpyrazolyl)borate
VE	valence electron
WT	wingtip

Figure Titles

Fig.1 Comparison of the π symmetry orbitals of $[\text{C}_8\text{H}_8]^{2-}$ with those of $[\text{C}_8\text{H}_6]^{2-}$. The HOMO is π_5 . [10]

Fig. 2. Examples of the coordination modes of pentalene ligands.

Fig. 3. Pentalene numbering system and geometric parameters for an η^8 -bound pentalene complex (a) fold angle, FA (b) twist angle, θ , for bis(pentalene) complexes.

Fig. 4. Correlation diagram of the six highest occupied orbitals of Pn_2Ti as function of θ . Reproduced with permission from [24]

Fig. 5. Frontier orbitals of ZrPn_2 and ThPn_2 with D_{2d} and D_2 symmetry. [10].

Fig. 6. Definition of Cartesian coordinates for a C_{2v} $\text{M}(\eta^8\text{-Pn})$ fragment.

Fig. 7. Energy levels and isosurfaces for the Kohn-Sham frontier orbitals of $\text{Zr}(\eta^8\text{-Pn})$ with C_{2v} symmetry.

Fig. 8. Isosurface for the HOMO of $(\eta^8\text{-Pn})\text{VCp}$. [10, 27]

Fig. 9. Definition of geometric parameters for ring slippage (Δ) and hinge angle (HA).

Fig. 10. Examples of di-metal bis(pentalene) double-sandwich complexes.

Fig. 11a. MO scheme for V_2Pn_2 built from V_2 and Pn fragments. [10]

Fig. 11b. Iso-surfaces for occupied orbitals of V_2Pn_2 with greater than 10% V occupancy. [10]

Fig. 12. MO energy levels for M_2Pn^*_2 ($\text{M}=\text{V-Ni}$) showing trend across the series and additional MO isosurfaces. [10, 60, 61]

Fig. 13. Ball and stick diagram of solid-state structure of Mn_2Pn^+_2 , constructed from published coordinates. H atoms and $i\text{Pr}$ groups omitted for clarity.

Fig. 14. M–M bond orders predicted by assuming that the bridging pentalene is a 5 electron L_2X donor to each metal; the allyl portion is an LX donor. The M–M bond orders predicted by this method are in accord with theory. Pentalene substituents are not shown for clarity. Adopted from ref [12].

Fig. 15. Examples of *anti*-bimetallic pentalene complexes. [72, 73, 77, 78]

Fig. 16. Frontier orbitals of a M_2Pn fragment. The higher lying orbitals $13b_u$ - $12a_g$ provide six orbitals that are available for bonding further ligands, the lower energy orbitals $6a_u$ to $10a_g$ correspond to t_{2g} sets of orbitals on each metal. They

house 12 metal d electrons and may be employed in back-bonding to further ligands.[10]

Fig. 17. Isosurfaces for the $11a_u$ and $11b_g$ orbitals of $\text{Fe}_2\text{PnCp}_2^{n+}$. [10]

Fig 18. Isosurfaces for the σ , π and δ V–V bonding orbitals of V_2PnCp_2 . [10]

Fig. 19. Isosurface for the HOMO of $\text{Fe}_2\text{Pn}^*(\text{CO})_5$ showing back donation to the bridging carbonyl ligand. [10]

Fig. 20. HOMO for $\text{Rh}_2\text{Pn}^*(\text{CO})_4$ (the Ir analogue has a similar HOMO and the Co analogue a similar HOMO-1). [10]

Fig. 21. Isosurface for the SOMO of PnFeCp . [3, 10]

Fig. 22. Calculated structure of Pn_2Fe . [10]

Fig. 23. Examples of mononuclear η^5 -pentalene complexes. [84-86]

Fig. 24. Ti–Ti bonding orbitals and back-donation orbitals to the CO groups for $\text{Pn}_2\text{Ti}_2(\text{CO})_n$, $n=1-3$. [40]

Fig. 25. Free energies for binding of CO_2 to Pn_2Ti_2 and the decomposition of $\text{Pn}_2\text{Ti}_2(\text{CO}_2)$ under dynamic vacuum. ADF (BP/TZP) values are given in red and Gaussian (B3LYP/SDD) values in black. Adapted from [41]

Fig. 26. The bonding orbital resulting from nucleophilic attack by Ti_2Pn_2 on CO_2 . [40]

Fig. 27. Structure-bonding representation of CO_2 binding in μ -Z fashion to $\text{Ti}_2\text{Pn}^\dagger_2$. $\text{R} = \text{Si}^i\text{Pr}_3$. [40, 94]

Fig. 28. Examples of group 4 pentalene complexes tested for olefin polymerisation activity. [97]

Fig. 29. Possible diastereomers of $\text{Pn}^*(\text{H})\text{ML}_3$ for non-chiral L.

Fig. 30. Examples of anti-bimetallic complexes studied for metal-metal interactions.

Fig. 31. Examples of hetero-bimetallics with asymmetric ligand environments.

References

- [1] F.G.N. Cloke, *Pure Appl. Chem.*, 73 (2001) 233–238.
- [2] O.T. Summerscales, F.G.N. Cloke, *Coord. Chem. Rev.*, 250 (2006) 1122–1140.
- [3] S. Bendjaballah, S. Kahlal, K. Costuas, E. Bévilion, J.-Y. Saillard, *Chem.–Eur. J.*, 12 (2006) 2048–2065.
- [4] J.W. Armit, R.V. Robinson, *J. Chem. Soc.*, 121 (1922) 827–839.
- [5] H.C. Longuet-Higgins, *Theoretical Organic Chemistry; Kekule Symposium*, Butterworths, London, 1959.
- [6] T. Bally, S. Chai, M. Neuenschwander, Z. Zhu, *J. Am. Chem. Soc.*, 119 (1997) 1869–1875.
- [7] P. De Mayo, R. Bloch, R.A. Marty, *J. Am. Chem. Soc.*, 93 (1971) 3071–3072.
- [8] E. Le Goff, *J. Am. Chem. Soc.*, 84 (1962) 3975–3976.
- [9] K. Hafner, H.U. Süss, *Angew. Chem. Int. Ed. Engl.*, 12 (1973) 575–577.
- [10] J.C. Green, Calculations carried out for the purposes of this review. ADF2014.01 BP/TZP/Zora level (<https://www.scm.com/>) (2016).
- [11] M.L.H. Green, *J. Organomet. Chem.*, 500 (1995) 127–148.
- [12] J.C. Green, M.L.H. Green, G. Parkin, *Chem. Commun.*, 48 (2012) 11481–11503.
- [13] R.D. Shannon, *Acta. Crystallogr. Sect. A.*, 32 (1976) 751–767.
- [14] F.M. Chadwick, R.T. Cooper, A.E. Ashley, J.C. Buffet, D. O'Hare, *Organometallics*, 33 (2014) 3775–3785.
- [15] F.G.N. Cloke, P.B. Hitchcock, M.C. Kuchta, N.A. Morley-Smith, *Polyhedron*, 23 (2004) 2625–2630.
- [16] K. Jonas, P. Kolb, G. Kollbach, B. Gabor, *Angew. Chem. Int. Ed. Engl.*, 36 (1997) 1714–1718.
- [17] A.E. Ashley, D.Phil Thesis, University of Oxford, 2006.
- [18] F.M. Chadwick, R.T. Cooper, D. O'Hare, *Organometallics*, 35 (2016) 2092–2100.
- [19] R.T. Cooper, F.M. Chadwick, A.E. Ashley, D. O'Hare, *Organometallics*, 32 (2013) 2228–2233.
- [20] F.G.N. Cloke, P.B. Hitchcock, *J. Am. Chem. Soc.*, 119 (1997) 7899–7900.
- [21] F.M. Chadwick, A. Ashley, G. Wildgoose, J.M. Goicoechea, S. Randall, D. O'Hare, *Dalton Trans.*, 39 (2010) 6789–6793.
- [22] G. Balazs, F.G.N. Cloke, J.C. Green, R.M. Harker, A. Harrison, P.B. Hitchcock, C.N. Jardine, R. Walton, *Organometallics*, 26 (2007) 3111–3119.
- [23] A. Ashley, G. Balazs, A. Cowley, J. Green, C.H. Booth, D. O'Hare, *Chem. Commun.*, (2007) 1515–1517.
- [24] R. Gleiter, S. Bethke, J. Okubo, K. Jonas, *Organometallics*, 20 (2001) 4274–4278.
- [25] G. Parkin, Classification of Organotransition Metal Compounds, in: R.H. Crabtree, D.M.P. Mingos (Eds.) *Comprehensive Organometallic Chemistry III*, Elsevier, Oxford, 2006, pp. 1–57.
- [26] Z.R. Turner, J.-C. Buffet, D. O'Hare, Patent App., 2016.
- [27] K. Costuas, J.-Y. Saillard, *Chem. Commun.*, (1998) 2047–2048.
- [28] F.G.N. Cloke, J.C. Green, C.N. Jardine, *Organometallics*, 18 (1999) 1087–1090.
- [29] J.P. Clark, J.C. Green, *Journal of the Chemical Society Dalton Transactions*, (1977) 505–508.

- [30] J.G. Brennan, J.C. Green, C.M. Redfern, *J. Am. Chem. Soc.*, 111 (1989) 2373-2377.
- [31] J.C. Green, M.P. Payne, A. Streitwieser Jr., *Organometallics*, 2 (1983) 1707-1710.
- [32] O. Mooßen, M. Dolg, *Chem. Phys. Lett.*, 594 (2014) 47-50.
- [33] M. Dolg, O. Mooßen, *J. Organomet. Chem.*, 794 (2015) 7-22.
- [34] J.C. Green, M.L.H. Green, C.K. Prout, *J. Chem. Soc. Chem. Commun.*, (1972) 421-422.
- [35] J.W. Lauher, R. Hoffmann, *J. Am. Chem. Soc.*, 98 (1976) 1729-1742 and references therein.
- [36] J.C. Green, *Chem. Soc. Rev.*, 27 (1998) 263-271.
- [37] H. Li, B. Wei, L. Xu, W.-X. Zhang, Z. Xi, *Angew. Chem. Int. Ed. Engl.*, 52 (2013) 10822-10825.
- [38] A.F.R. Kilpatrick, PhD Thesis, University of Sussex, 2014.
- [39] K. Jonas, P. Kolb, G. Kollbach, US Pat. 5959132 A, 1999.
- [40] A.F.R. Kilpatrick, J.C. Green, F.G.N. Cloke, *Organometallics*, 34 (2015) 4830-4843.
- [41] A.F.R. Kilpatrick, J.C. Green, F.G.N. Cloke, *Organometallics*, 34 (2015) 4816-4829.
- [42] R.T. Cooper, F.M. Chadwick, A.E. Ashley, D. O'Hare, *Chem. Commun.*, (2015) 1856-1859.
- [43] A.F.R. Kilpatrick, F.G.N. Cloke, *Chem. Commun.*, 50 (2014) 2769-2771.
- [44] A.F.R. Kilpatrick, J.C. Green, F.G.N. Cloke, Manuscript in preparation.
- [45] D.A.X. Fraser, Z.R. Turner, J.-C. Buffet, D. O'Hare, *Organometallics*, 35 (2016) 2664-2674.
- [46] B. Gabor, K. Jonas, R. Mynott, *Inorg. Chim. Acta*, 270 (1998) 555-558.
- [47] A.F.R. Kilpatrick, J.C. Green, F.G.N. Cloke, N. Tsoureas, *Chem. Commun.*, 49 (2013) 9434-9436.
- [48] K. Jonas, B. Gabor, R. Mynott, K. Angermund, O. Heinemann, C. Krüger, *Angewandte Chemie International Edition in English*, 36 (1997) 1712-1714.
- [49] Q.A. Abbasali, F.G.N. Cloke, P.B. Hitchcock, S.C.P. Joseph, *Chem. Commun.*, (1997) 1541-1542.
- [50] F.G.N. Cloke, P.B. Hitchcock, *J. Am. Chem. Soc.*, 124 (2002) 9352.
- [51] J.H. Farnaby, F.G.N. Cloke, M.P. Coles, J.C. Green, G. Aitken, *C. R. Chim.*, 13 (2010) 812-820.
- [52] O.T. Summerscales, D.R. Johnston, F.G.N. Cloke, P.B. Hitchcock, *Organometallics*, 27 (2008) 5612-5618.
- [53] F.M. Chadwick, D.M. O'Hare, *Organometallics*, 33 (2014) 3768-3774.
- [54] T.J. Katz, N. Acton, J. McGinnis, *J. Am. Chem. Soc.*, 94 (1972) 6205-6206.
- [55] T.J. Katz, N. Acton, *J. Am. Chem. Soc.*, 94 (1972) 3281-3283.
- [56] G. Balazs, F.G.N. Cloke, L. Gagliardi, J.C. Green, A. Harrison, P.B. Hitchcock, A.R.M. Shahi, O.T. Summerscales, *Organometallics*, 27 (2008) 2013-2020.
- [57] M.C. Kuchta, F.G.N. Cloke, P.B. Hitchcock, *Organometallics*, 17 (1998) 1934-1936.
- [58] A.D. Smith, F.G.N. Cloke, Unpublished results.
- [59] O.T. Summerscales, C.J. Rivers, M.J. Taylor, P.B. Hitchcock, J.C. Green, F.G.N. Cloke, *Organometallics*, 31 (2012) 8613-8617.
- [60] A.E. Ashley, R.T. Cooper, G.G. Wildgoose, J.C. Green, D. O'Hare, *J. Am. Chem. Soc.*, 130 (2008) 15662-15677.

- [61] S.C. Binding, J.C. Green, W.K. Myers, D. O'Hare, *Inorg. Chem.*, 54 (2015) 11935-11940.
- [62] F.G.N. Cloke, J.C. Green, C.N. Jardine, M.C. Kuchta, *Organometallics*, 18 (1999) 1087-1090.
- [63] G. Balazs, F.G.N. Cloke, A. Harrison, P.B. Hitchcock, J. Green, O.T. Summerscales, *Chem. Commun.*, (2007) 873-875.
- [64] S.C. Jones, D. O'Hare, *Chem. Commun.*, (2003) 2208-2209.
- [65] S.C. Jones, T. Hascall, A.J. Norquist, D. O'Hare, *Inorg. Chem.*, 42 (2003) 7707-7709.
- [66] S.C. Jones, T. Hascall, S. Barlow, D. O'Hare, *J. Am. Chem. Soc.*, 124 (2002) 11610-11611.
- [67] D.F. Hunt, J. Russell, *J. Organomet. Chem.*, 46 (1972) C22-C24.
- [68] D.F. Hunt, J. Russell, *J. Am. Chem. Soc.*, 94 (1972) 7198-7199.
- [69] W. Weidermuller, K. Hafner, *Angew. Chem. Int. Ed. Engl.*, 12 (1973) 925.
- [70] A.E. Ashley, G. Balazs, A.R. Cowley, J.C. Green, D. O'Hare, *Organometallics*, 26 (2007) 5517-5521.
- [71] A. Brookes, F. Gordon, J. Howard, S.A.R. Knox, P. Woodward, *J. Chem. Soc. Chem. Commun.*, (1973) 587-589.
- [72] E.E. Bunel, L. Valle, N.L. Jones, P.J. Carroll, C. Barra, M. Gonzalez, N. Munoz, G. Visconti, A. Aizman, J.M. Manríquez, *J. Am. Chem. Soc.*, 110 (1988) 6596-6598.
- [73] J.M. Manríquez, M.D. Ward, W.M. Reiff, J.C. Calabrese, N.L. Jones, P.J. Carroll, E.E. Bunel, J.S. Miller, *J. Am. Chem. Soc.*, 117 (1995) 6182-6193.
- [74] A.F.R. Kilpatrick, D.R. Johnston, J.C. Green, N. Tsoureas, M.P. Coles, F.G.N. Cloke, *Polyhedron*, (2016) DOI: 10.1016/j.poly.2016.1003.1001.
- [75] S.C. Binding, D.Phil Thesis, University of Oxford, 2015.
- [76] F.M. Chadwick, A.E. Ashley, R.T. Cooper, L.A. Bennett, J.C. Green, D.M. O'Hare, *Dalton Trans.*, 44 (2015) 20147-20153.
- [77] A. Miyake, A. Kanai, *Angew. Chem. Int. Ed. Engl.*, 10 (1971) 801-802.
- [78] Y. Kitano, M. Kashiwagi, Y. Kinoshita, *Bull. Chem. Soc. Jpn.*, 46 (1973) 723-727.
- [79] O.T. Summerscales, S.C. Jones, F.G.N. Cloke, P.B. Hitchcock, *Organometallics*, 28 (2009) 5896-5908.
- [80] A.F.R. Kilpatrick, F.G.N. Cloke, N. Tsoureas, *Dalton Trans.*, Manuscript submitted.
- [81] M.T. Garland, J.-Y. Saillard, I. Chávez, B. Oelckers, J.M. Manríquez, *J. Mol. Struct. Theochem*, 390 (1995) 199-208.
- [82] T.J. Katz, M. Rosenberger, *J. Am. Chem. Soc.*, 85 (1963) 2030-2031.
- [83] E. Molins, W. Maniukiewicz, C. Miravittles, M. Mas, J.M. Manríquez, I. Chávez, B. Oelckers, J. Farran, J.L. Brianso, *Acta Crystallogr., Sect. C: Cryst. Struct. Commun.*, 52 (1996) 2414-2416.
- [84] K. Jonas, K.R. Porschke, 224th ACS National Meeting, 2002.
- [85] K. Jonas, Report for the Period of January 2000 - December 2001, Max-Planck-Institut für Kohlenforschung, (2002).
- [86] K. Jonas, Report for the Period of January 2002 - December 2004, Max-Planck-Institut für Kohlenforschung, (2005).
- [87] M. Aresta, *Carbon Dioxide as Chemical Feedstock*, Wiley, 2010.
- [88] G.A. Olah, *Angew. Chem. Int. Ed. Engl.*, 44 (2005) 2636-2639.
- [89] W.B. Tolman, *Activation of Small Molecules: Organometallic and Bioinorganic Perspectives*, Wiley VCH, 2007.

- [90] K.P. Huber, G. Herzberg, *Molecular Spectra and Molecular Structure. IV. Constants of Diatomic Molecules*, Van Nostrand Reinhold Co, 1979.
- [91] F.G.N. Cloke, J.C. Green, N. Kaltsoyannis, *Organometallics*, 23 (2004) 832-835.
- [92] N. Tsoureas, A.F.R. Kilpatrick, O.T. Summerscales, J.F. Nixon, F.G.N. Cloke, P.B. Hitchcock, *Eur. J. Inorg. Chem.*, (2013) 4085-4089.
- [93] O.T. Summerscales, F.G.N. Cloke, P.B. Hitchcock, J.C. Green, N. Hazari, *Science*, 311 (2006) 829-831.
- [94] A. Paparo, J. Okuda, *Coord. Chem. Rev.*, (2016) DOI: 10.1016/j.ccr.2016.1006.1005.
- [95] R.T. Cooper, D.Phil Thesis, University of Oxford, 2012.
- [96] A. Andresen, H.-G. Cordes, J. Herwig, W. Kaminsky, A. Merck, R.P. Mottweiler, J. , H. Sinn, H.-J. Vollmer, *Angew. Chem. Int. Ed. Engl.*, 88 (1976) 689-690.
- [97] H. Sinn, W. Kaminsky, *Adv. Organomet. Chem.*, 18 (1980) 99-149.
- [98] H.G. Alt, A. Köppl, *Chem. Rev.*, 100 (2000) 1205-1222.
- [99] G.W. Coates, *Journal of the Chemical Society Dalton Transactions*, (2002) 467-475.
- [100] B. Cornils, W.A. Herrmann, M. Beller, R.A. Paciello, *Applied Homogeneous Catalysis with Organometallic Compounds: A Comprehensive Handbook in Three Volumes*, 3rd ed., Wiley VCH, 2012.
- [101] W. Kaminsky, *Polyolefins: 50 years after Ziegler and Natta*, Springer, Berlin, 2013.
- [102] G.J. Britovsek, V.C. Gibson, D.F. Wass, *Angew. Chem. Int. Ed. Engl.*, 38 (1999) 428-447.
- [103] F.G.N. Cloke, J.S. Parry, Patent App. WO1999007716 A1, 1999.
- [104] E.Y. Chen, T.J. Marks, *Chem. Rev.*, 100 (2000) 1391-1434.
- [105] J.-C. Buffet, Z.R. Turner, R.T. Cooper, D. O'Hare, *Polym. Chem.*, 6 (2015) 2493-2503.
- [106] B.-H. Xu, G. Kehr, R. Fröhlich, E. Nauha, G. Erker, *Dalton Trans.*, 39 (2010) 9973-9981.
- [107] G.G. Hlatky, *Coord. Chem. Rev.*, 181 (1999) 243-296.
- [108] F. Helmer-Metzmann, F. Osan, M. Riedel, Patent App. CA2179355 A1, 1996.
- [109] F. Burgos, I. Chávez, J. Manríquez, *Organometallics*, 20 (2001) 1287-1291.
- [110] F. Burgos, V. Arancibia, J.M. Manríquez, I. Chávez, *Bol. Soc. Chil. Quím.*, 45 (2000) 621-628.
- [111] R.M. Bullock, C.P. Casey, *Acc. Chem. Res.*, 20 (1987) 167-173.
- [112] D.W. Stephan, *Coord. Chem. Rev.*, 95 (1989) 41-107.
- [113] N. Wheatley, P. Kalck, *Chem. Rev.*, 99 (1999) 3379-3420.
- [114] L. Gade, *Angew. Chem. Int. Ed. Engl.*, 39 (2000) 2658-2678.
- [115] V. Ritleng, M.J. Chetcuti, *Chem. Rev.*, 107 (2007) 797-858.
- [116] M. Shibasaki, Y. Yamamoto, *Bimetallic Catalysts in Organic Synthesis Chemistry*, Wiley VCH, 2004.
- [117] J.I. van der Vlugt, *Eur. J. Inorg. Chem.*, 2012 (2011) 363-375.
- [118] B.G. Cooper, J.W. Napoline, C.M. Thomas, *Catal. Rev.*, 54 (2012) 1-40.
- [119] Z.R. Turner, J.-C. Buffet, D. O'Hare, *Organometallics*, 33 (2014) 3891-3903.
- [120] S. Barlow, D. O'Hare, *Chem. Rev.*, 97 (1997) 637-667.
- [121] T.J. Peckham, P. Gbmez-Elipe, I. Manners, *Metallocene-Based Polymers*, in: A. Togni, R.L. Halterman (Eds.) *Metallocenes*, Wiley-VCH Verlag GmbH, 2008, pp. 723-772.

- [122] M.B. Robin, P. Day, *Adv. Inorg. Chem. Radiochem.*, 10 (1967) 247-422.
- [123] P. Day, N.S. Hush, R.J.H. Clark, *Philos. Trans. R. Soc. A*, 366 (2008) 5-14.
- [124] P.J. Low, *Dalton Trans.*, (2005) 2821-2824.
- [125] J.E. Sutton, H. Taube, *Inorg. Chem.*, 20 (1981) 3125-3134.
- [126] B. Oelckers, I. Chávez, J.M. Manríquez, *Organometallics*, 12 (1993) 3396.
- [127] Y. Portilla, I. Chávez, V. Arancibia, B. Loeb, J.M. Manríquez, A. Roig, E. Molins, *Inorg. Chem.*, 41 (2002) 1831-1836.
- [128] M.B. Robin, P. Day, *Mixed Valence Chemistry-A Survey and Classification*, Elsevier, 1968.
- [129] J.J. Le Roy, M. Jeletic, S.I. Gorelsky, I. Korobkov, L. Ungur, L.F. Chibotaru, M. Murugesu, *J. Am. Chem. Soc.*, 135 (2013) 3502-3510.
- [130] N. Magnani, C. Apostolidis, A. Morgenstern, E. Colineau, J.-C. Griveau, H. Bolvin, O. Walter, R. Caciuffo, *Angew. Chem. Int. Ed. Engl.*, 50 (2011) 1696-1698.
- [131] G.A. Molander, J.A.C. Romero, *Chem. Rev.*, 102 (2002) 2161-2186.
- [132] S. Kobayashi, M. Sugiura, H. Kitagawa, W.W.-L. Lam, *Chem. Rev.*, 102 (2002) 2227-2302.
- [133] A.M. Nonat, S.J. Quinn, T. Gunnlaugsson, *Inorg. Chem.*, 48 (2009) 4646-4648.
- [134] S. Marks, J.G. Heck, M.H. Habicht, P. Oña-Burgos, C. Feldmann, P.W. Roesky, *J. Am. Chem. Soc.*, 134 (2012) 16983-16986.
- [135] W. Reiff, J.M. Manríquez, J.S. Miller, *Abstracts of Papers of the American Chemical Society*, 1989.
- [136] W. Reiff, J.M. Manríquez, J.S. Miller, *Hyperfine Interact.*, 53 (1990) 397-402.
- [137] W. Reiff, J.M. Manríquez, M. Ward, J.S. Miller, *Mol. Cryst. Liquid Cryst.*, 176 (1989) 423-428.
- [138] Y. Matsuura, K. Matsukawa, *Chem. Phys. Lett.*, 453 (2008) 92-96.
- [139] Y. Matsuura, *Solid State Commun.*, 151 (2011) 1877-1880.
- [140] C.J. Rivers, *D.Phil Thesis, University of Sussex*, 2004.
- [141] S.C. Jones, *D.Phil Thesis, University of Oxford*, 2003.